Plant Biotechnology Journal Open Access

Plant Biotechnology Journal (2025) **23**, pp. 3540–3560 doi: 10.1111/pbi.70149

Modulating the activity of the APC/C regulator SISAMBA improves the sugar and antioxidant content of tomato fruits

Perla Novais de Oliveira[1], Leonardo Perez de Souza[2], Pedro Boscariol Ferreira[1], Jean Phillippe Mauxion[3], Luis Felipe Correa da Silva[1], Ana Isabela Chang[1], Marina de Lyra Soriano Saleme[1], Feng Zhu[2,4], Sara Selma García[5,6], Herman De Beukelaer[5,6], Marina C. M. Martins[7], Laise Rosado-Souza[2], Lilian Ellen Pino[1], Norbert Bollier[3], Lázaro Eustáquio Pereira Peres[1], Klaas Vandepoele[5,6], Alain Goossens[5,6,8], Nathalie Gonzalez[3], Alisdair R. Fernie[2] and Nubia Barbosa Eloy[1,*]

[1]*Departamento de Ciências Biológicas, Escola Superior de Agricultura 'Luiz de Queiroz' (ESALQ), University of São Paulo (USP), Piracicaba, Brazil*
[2]*Max-Planck-Institute of Molecular Plant Physiology, Potsdam-Golm, Germany*
[3]*INRAE, UMR1332 Biologie du Fruit et Pathologie, Université Bordeaux, Villenave d'Ornon, France*
[4]*National Key Laboratory for Germplasm Innovation & Utilization of Horticultural Crops, Huazhong Agricultural University, Wuhan, China*
[5]*Department of Plant Biotechnology and Bioinformatics, Ghent University, Ghent, Belgium*
[6]*VIB Center for Plant Systems Biology, Ghent, Belgium*
[7]*in Press Consultoria e Comunicação Científica, São Paulo, Brazil*
[8]*Department of Botany and Zoology, Stellenbosch University, Matieland, South Africa*

Received 30 December 2024;
revised 5 May 2025;
accepted 12 May 2025.
**Correspondence* (Tel +55 (19) 3429-4117 +55 (19) 3429-4268; fax +55 (19) 3447-8649; email nbeloy@usp.br)

Keywords: APC/C, CRISPR/Ca9, fruit development, metabolic changes, tomato, transcriptomic analysis.

Summary

The Anaphase-Promoting Complex/Cyclosome (APC/C) is an E3 ubiquitin ligase that plays a crucial role in ubiquitin-dependent proteolysis of key cell cycle regulators, which is completed by the 26S proteasome. Previously, SAMBA, a plant-specific regulator of the APC/C, was identified in Arabidopsis as a critical factor controlling organ size through the regulation of cell proliferation. Here, by assessing its role in the crop tomato (*Solanum lycopersicum*), we confirm that SAMBA is a conserved APC/C regulator in plants and shows additional roles, including the modulation of fruit shape and changes in sugar metabolism. Two *slsamba* genome-edited lines were produced and characterized, and showed delayed growth, reduced plant size, and altered fruit morphology, which were linked to changes in cell division and expansion. Notably, untargeted metabolomics revealed altered flavonoid profiles, along with elevated Brix values in the fruits, indicating a sweeter taste. Accordingly, transcriptomics uncovered a change in temporal gene expression gradients during early fruit development, correlating with the alterations in sugar metabolism and revealing changes in cell wall biosynthesis genes. This study provides the first evidence of *SAMBA's* role in regulating fruit development, metabolic content, and ultimately, quality. These important findings offer potential applications for improving the nutritional quality and overall performance of tomatoes.

Introduction

Cell cycle progression must be precisely regulated to achieve proper plant growth, organ development, and reproduction. This process requires the coordinated destruction of essential cell cycle regulatory proteins by specific E3 ubiquitin ligases, known as Anaphase-Promoting Complex/Cyclosome (APC/C) and SKP1-Cullin1-F-box (SCF) complexes that recognize proteins to be polyubiquitinated and subjected to proteolysis by the 26S proteasome. The SCF complex is crucial at the G1 to S transition phase, where it targets cell cycle-dependent kinase inhibitors (CKIs), including Substrate/Subunit Inhibitor of Cyclin-dependent protein kinase (SIC1) in yeast (Dirick *et al.*, 1995) and Kip-related proteins (KRPs) in plants (Ren *et al.*, 2008; Verkest *et al.*, 2005). In contrast, the APC/C complex primarily functions at the G2 to M transition and mitotic exit. In all organisms, for these two transitions, mitotic cyclins and securin must be targeted for degradation by the APC/C (Buschhorn and Peters, 2006; Capron *et al.*, 2003; Harper *et al.*, 2002; Petersen *et al.*, 2000). Although the functions of these multi-protein machines have been primarily investigated in *Arabidopsis thaliana*, other plant species remain less explored. Hence, understanding the importance of these complexes in crops such as tomato can reveal unique regulatory mechanisms and potential applications in agriculture and biotechnology, enhancing the translatability of basic research findings for crop improvement (Inzé and Nelissen, 2022).

The APC/C in plants can comprise up to 14 subunits, such as in Arabidopsis, maize, and sorghum, which are divided into at least three main functional modules: a catalytic/substrate recognition module (APC2, APC11, and APC10), a structural module (APC3, APC6, APC7, and APC8) (Alfieri *et al.*, 2017; D'Andrea and Regan, 2003), and a scaffolding module to which the catalytic and structural components are attached (APC1, APC4, and APC5)

(Alfieri *et al*., 2017; Eloy *et al*., 2015; Thornton *et al*., 2006; Thornton and Toczyski, 2003). Moreover, the APC/C activity is regulated by two structurally related co-activator proteins, CELL DIVISION CYCLE 20 (CDC20) and CELL CYCLE SWITCH 52 (CCS52) (Baker *et al*., 2007; Peters, 2002), and inhibited by ULTRAVIOLET-B-INSENSITIVE4 (UVI4) and its homologue OMISSION OF SECOND DIVISION 1 (OSD1)/GIGAS CELL 1 (GIGAS)/UVI4-Like (d'Erfurth *et al*., 2009; Heyman *et al*., 2011; Iwata *et al*., 2011).

Functional characterization of APC/C subunits in Arabidopsis has revealed their essential roles in cell differentiation, development of the shoot and root meristems, plant growth, vascular development, hormone regulation, and endoreduplication (Blilou *et al*., 2002; Eloy *et al*., 2011, 2012; Marrocco *et al*., 2009; Rojas *et al*., 2009; Saze and Kakutani, 2007; Schwedersky *et al*., 2021). In *Medicago truncatula*, the APC6 regulates the number of lateral roots and nodule formation (Kuppusamy *et al*., 2009). In *Oryza sativa*, APC6 knockout plants show reduced height and smaller cell size, while the *Tiller Enhancer* (*TE*) gene, a homologue of CCS52A, controls shoot branching and tillering (Kumar *et al*., 2010; Lin *et al*., 2012).

Previously, we have identified a plant-specific APC/C regulator named SAMBA (Eloy *et al*., 2012). Loss-of-function mutation of *SAMBA* in Arabidopsis led to increased cell proliferation, resulting in larger leaves, roots, and seeds. In maize, Clustered Regularly Interspaced Palindromic Repeats/CRISPR-associated protein 9 (CRISPR/Cas9) *zmsamba* mutants also show an increased rate of cell division. However, these plants displayed reduced organ and tissue growth, resulting in dwarfism as a consequence of decreased cell size (Gong *et al*., 2022). Besides these contrasting phenotypes, the *SAMBA* expression pattern also varies between these species during development. In Arabidopsis, *SAMBA* is highly expressed during embryogenesis, with transcripts gradually decreasing when seedlings germinate, being restricted to the hypocotyl at 8 days after stratification (DAS), and exclusively detected in pollen grains at more advanced developmental stages. By contrast, *ZmSAMBA* expression in maize is relatively constant throughout the entire development (Sekhon *et al*., 2011).

Here, we identified and investigated the role of *SlSAMBA* in tomato plants, an excellent model for studying fleshy fruit development. Tomato is particularly interesting due to its significant economic value, short life cycle, the availability of extensive genomic resources, and the established protocols for genetic manipulation (Zhang *et al*., 2016). After pollination, tomato fruits undergo a very orchestrated growth journey, progressing through successive and overlapping phases of cell division, expansion, and ripening (Mauxion *et al*., 2021; Mumtaz *et al*., 2022). The growth period during which cell proliferation, cell expansion, and endoreduplication will determine final fruit size is accompanied by important metabolic changes, leading to the formation of mature tomato fruits rich in structurally diverse metabolites. The consumption of tomatoes has been associated with health benefits, including a lower incidence of several chronic diseases and certain types of cancer (Giovannucci, 1999; Willcox *et al*., 2003), which are often attributed to the high levels of antioxidant secondary compounds, particularly flavonoids, that accumulate in the fruit (Martin and Li, 2017; Zhang *et al*., 2015).

To gain a deeper understanding of *SlSAMBA*'s functional role, we employed CRISPR/Cas9-based genome editing to generate *SlSAMBA* loss-of-function plants (*slsamba*) in the Micro-Tom tomato. These mutants exhibited delayed growth and altered development demonstrated by reductions in both plant size and fruit dimensions. Alterations in fruit morphology, particularly a shift towards elongated shapes and impaired seed set, suggest that SlSAMBA plays a critical role in regulating pistil/ovary development, as well as reproductive success in tomato plants. Moreover, metabolic profiling identified higher contents of soluble sugars and compounds related to flavonoids in the *slsamba* fruits. These combined results show that SlSAMBA plays a key role in regulating various aspects of tomato fruit development, with potential implications for improving crop quality.

Results

The tomato genome contains the SAMBA gene, which is highly expressed in the early stages of flower and fruit development

The Arabidopsis SAMBA (AT1G32310) protein contains three putative motifs (SHR1, LCR, and SHR2) previously identified by Eloy *et al*. (2012), which appear to be conserved across most plant species (Figure 1a). Our search for a SAMBA homologue in tomato identified a single gene, *Solyc08g076580.2* (hereafter referred to as *SlSAMBA*). The open reading frame of *SlSAMBA* has 342 base pairs (bp) and encodes a 113-amino acid protein. Our phylogenetic analysis shows that SlSAMBA protein is closely related to its counterpart in tobacco (Figure 1a) and multiple sequence alignment reveals high similarity to other homologues (Figure 1b). Data from the general feature format (GFF) file provided with the genome sequence revealed that the *SlSAMBA* gene is located at the end of the long arm of chromosome 8.

We assessed the mRNA levels of *SlSAMBA* in different organs and developmental stages by quantitative reverse transcriptase PCR (qRT-PCR) (Figure 1c). *SlSAMBA* showed the highest expression in floral buds (20 days before anthesis −20 DBA) and −1 DBA, which decreased in flowers at anthesis (0 days post anthesis – DPA). In the fruit, *SlSAMBA* was more expressed at 10 DPA compared to 20 DPA and the red ripe stage (52 DPA). In 30-day-old plants, *SlSAMBA* transcripts were undetectable in the root but were present in the leaves, with higher levels in the early (first leaf) than in the later (fifth leaf) stages of development. Additionally, in silico analysis of public transcriptome data from Plant eFP (Waese *et al*., 2017) revealed that *SlSAMBA* is widely expressed in all organs (Figure S1), with higher expression levels during early developmental stages. This finding supports our qRT-PCR data and is consistent with the essential role of SlSAMBA in cell cycle regulation.

To further analyze the expression pattern of *SlSAMBA*, a 1.6-kb fragment upstream of its ATG start codon was cloned into the pKGWFS7 vector to drive the expression of β-glucuronidase/green fluorescent protein (GUS-GFP) reporters, and the construct (Figure S2a) was introduced into Micro-Tom tomato plants. *SlSAMBA* expression was particularly high during embryogenesis (Figure S2b) and was observed in different parts of the pistil, including the ovary and stigma, but not in the style (Figure 1d). In the androecium, *SlSAMBA* was expressed in both the anther and pollen grains, as shown in Figure 1d. During fruit development, the highest *SlSAMBA* expression occurred at 10 DPA, a phase known for intense cell division, and decreased

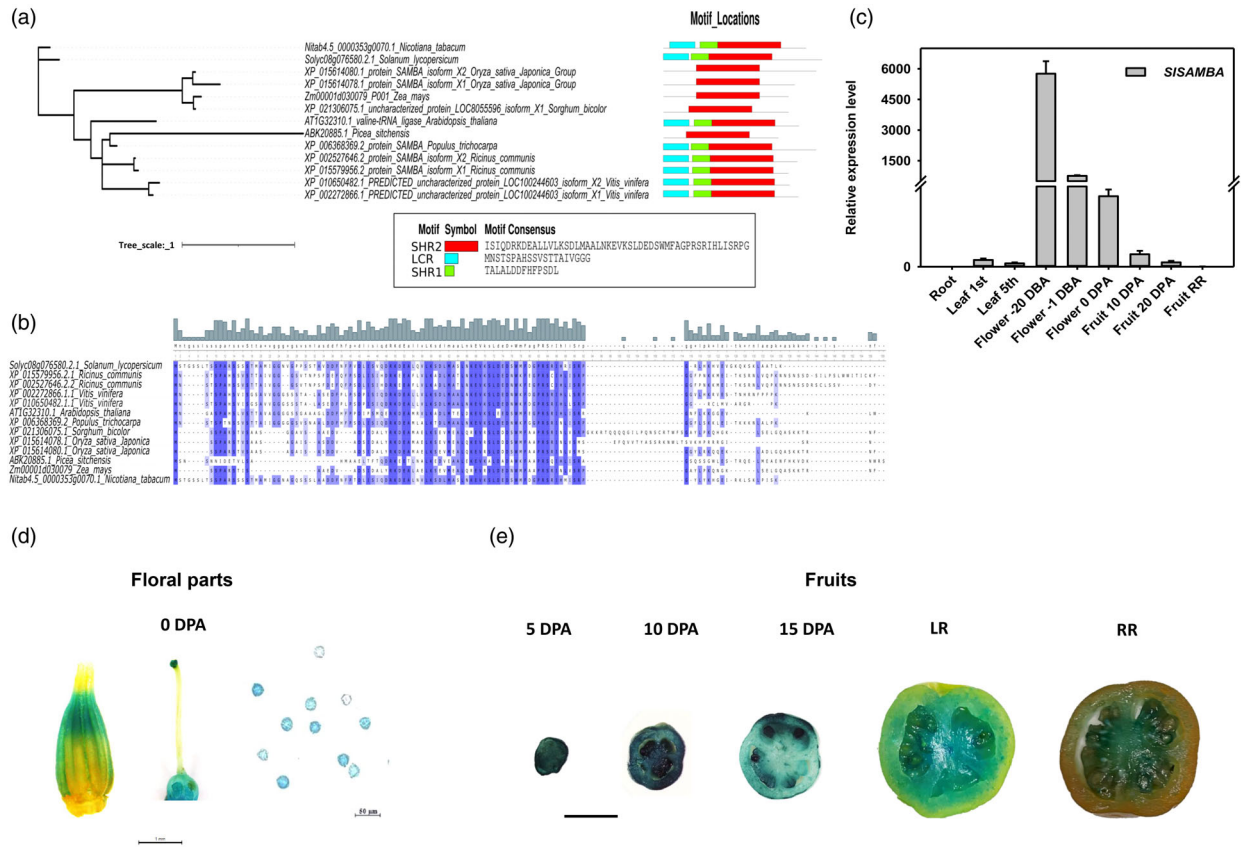

Figure 1 Phylogenetic relationships and architecture of conserved motifs in the SlSAMBA protein and spatio-temporal expression of *SlSAMBA* in tomato cv. Micro-Tom. (a) Phylogenetic tree of SAMBA proteins from *Solanum lycopersicum*, *Ricinus communis*, *Vitis vinifera*, *Arabidopsis thaliana*, *Populus trichocarpa*, *Sorghum bicolour*, *Oryza sativa*, *Picea sitchensis*, *Zea mays*, and *Nicotiana tabacum* constructed using IQ-Tree v.1.6.9. Three putative conserved motifs (SHR1, LCR, and SHR2) described by Eloy *et al*. (2012) were identified in most SAMBA homologues. Their location and motif consensus sequences are shown. (b) Multiple sequence alignment of the *S. lycopersicum Solyc08g076580.2.1* gene (SAMBA-homologue) was performed using Clustal X version 2.1 with default parameters (Thompson *et al*., 1997). (c) Tissue-specific expression profile of *SlSAMBA*. Data was generated by qRT-PCR, using *β-actin* as an internal control. Root (30-day-old plants), 1st leaf, and 5th leaf in logarithmic scale, with 26 to 500 on the x-axis omitted; 20 days before anthesis (−20 DBA), −1 DBA, flowers at the pre-anthesis stage, 1 day before anthesis; and 0 DPA, the day of anthesis; 10 DPA, 10 days post-anthesis, 20 DPA, 20 days post-anthesis; and RR, red ripe fruit. (d) *SlSAMBA* expression was high in the anther, pistil, and pollen grains. Scale bar = anther and pistil (1 mm), pollen grains (50 μm), and fruits (2 mm). (e) Flowers at anthesis, i.e. 0 days post-anthesis (0 DPA), and fruits at 5 DPA, 10 DPA, and 15 DPA, as well as at different maturity stages, i.e. light red (LR), and red ripe (RR). The *SlSAMBA* expression is higher at the early stages of fruit development.

afterwards until the ripening stage, when the expression was restricted to the septum and columella (Figure 1e).

SlSAMBA interacts with APC3b and APC6, two members of the APC/C complex

Several studies have shown that APC/C subunits have dynamic changes in localization, mainly exhibiting nuclear localization, with a lesser extent of presence in the cytoplasm (Blilou *et al*., 2002; Capron *et al*., 2003; Eloy *et al*., 2011; Wang *et al*., 2012; Guo *et al*, 2016). To determine the subcellular localization of SlSAMBA, we fused its N-terminal region with eGFP (Figure S2c,d). The eGFP-SlSAMBA fusion was transiently expressed in epidermal cells of 30-day-old tobacco leaves through Agrobacterium infiltration. The green fluorescence emission was detected in the nuclei, but it was also observed in the cytoplasm, confirming the *in silico* analyzes (Tables S1 and S2).

To identify protein interactors of SlSAMBA, we employed TurboID-mediated proximity labelling in tomato hairy roots (Arora *et al*., 2020). This approach is based on the *in planta* expression of the promiscuous biotin ligase TurboID fused to a target protein of interest, after which streptavidin-based affinity purification is used to capture the biotinylated proteins that (in)directly interact with or sit in proximity to the target protein. An advantage of the TurboID system is its ability to detect indirect interactions, which is useful for studying large protein complexes (Zhang *et al*., 2022). The SlSAMBA-TurboID fusion construct was stably expressed in tomato hairy roots and compared to controls to verify intact protein expression and (auto-)biotinylation activity of the TurboID-fusion proteins.

A total of 34 (at a permissive false discovery rate (FDR) of 0.01) or 16 (at a stringent FDR of 0.001) proteins were significantly enriched in the SlSAMBA-TurboID samples compared to the eGFP-TurboID controls (Data S1). Seven out of the 16 exhibited over fourfold enrichment (log_2) among these interacting or proximal proteins. Notably, two of the interactors were identified as tomato APC/C subunits APC6 and APC3b (Data S1; Figure S3a,

b), and another two as homologues of Arabidopsis NAP1-RELATED PROTEIN 2 (NRP2) involved in the cell cycle. This demonstrates that, as in other plant species, SlSAMBA is a member of the APC/C complex in tomato (Eloy *et al*., 2012).

To confirm the Turbo ID results, which showed that SISAMBA interacts with two core APC/C subunits in tomato, we performed a yeast two-hybrid (Y2H) assay. We tested the interaction of SISAMBA with SlAPC3b to validate the Turbo ID interaction and used SlAPC10 as a control to confirm the absence of interaction. Our results showed a direct interaction between SISAMBA and SlAPC3b (Figure S3c), which was consistent with our previous findings in Arabidopsis (Eloy *et al*., 2012).

SISAMBA frameshift mutants exhibit a dwarf phenotype with reduced organ size

We next used CRISPR/Cas9-based gene editing to induce mutations in *SlSAMBA* and characterize the phenotype of the edited plants. To obtain CRISPR-Cas9 *slsamba* mutants, a dual gRNA approach was used, employing two distinct gRNA combinations to transform tomato (Figure S4a). After sequencing 65 selected transformants, we identified two plants showing different mutations. The *slsamba*-27 mutant (construct 1) features a single nucleotide deletion at the first target site (gRNA3), resulting in a stop codon at positions 178–180 and potentially an in-frame deletion of 53 amino acids (Figure S4b,c). The *slsamba*-3 mutant (construct 2) carries a 73-nucleotide deletion between the two gRNAs (Figure S4b), resulting in a premature stop codon and potentially a shorter protein of 61 amino acids (Figure S4c). Alternatively, if the aberrant mRNA is degraded, no protein will be produced.

The two T0 *slsamba* mutants were backcrossed with wild-type (WT) and T1 heterozygous plants without the Cas9 sequence were selected and self-pollinated. In the fourth generation (T4), we obtained homozygous mutants, and qRT-PCR analysis of whole plants confirmed that both *slsamba* lines have very low relative expression levels of *SlSAMBA* compared to the WT (Figure S4d).

To assess the impact of the *slsamba* mutation on tomato development, we measured several growth-related parameters at both the vegetative and reproductive stages. The edited plants were dwarf (Figure 2a), with the height of the first inflorescence significantly shorter by 56.2% (line 3) and 46.9% (line 27) compared to the WT (Figure 2b). Additionally, they showed reduced stem diameter (Figure 2c) and a smaller leaf area (Figure 2d,e).

Since Arabidopsis *SAMBA* mutants exhibit defects in male gametophyte development (Eloy *et al*., 2012), we investigated whether similar phenotypic alterations were present in the tomato-edited lines. The *slsamba* mutants produced smaller flowers with thinner anthers at anthesis (Figure 2f,g). Furthermore, their mature fruits were more elongated and thinner compared to WT (Figure 2h,i), with reduced weight throughout development (Figure 2i,j). By measuring the fruit shape index, we found that the elongated fruit phenotype was evident as early as anthesis, and it was associated with a decrease in both weight and diameter (Figure S5).

Effect of *slsamba* mutation on female and male gametophytes

We observed that fruits from homozygous *slsamba* plants contained notably fewer seeds, with an average of 2.1 seeds per fruit (~8% of the average 26.1 from the WT) (Figure 3a). The reduced seed number suggests potential issues in gametogenesis, impairing pollination and seed formation. To explore this further, we analyzed the phenotypes of the flowers in detail, with particular focus on the ovary and pollen.

The pistil of *slsamba* mutants (lines 3 and 27) exhibited thinner stigma width and shorter style compared to WT plants at anthesis, but ovary length was not different at this stage (Figure 3b,c). Additionally, locule number quantification revealed that over 90% of the fruits from both edited lines contained two locules compared to the WT, which predominantly had three locules (Figure 3d). Pollen analysis showed low viability and germination rates in *slsamba* mutants, with only 9.5% (line 3) and 11.3% (line 27) of anthers being viable and 9.7% (line 3) and 12.8% (line 27) of pollen grains germinating. These results were partially explained by the aberrant morphology of pollen grains from the edited lines compared to WT pollen, as illustrated by the electron microscopy images shown in Figure 3e–g.

To pinpoint the effect of *slsamba* knockout on fruit phenotype, specifically fruit shape and seed formation, we conducted reciprocal crosses between *slsamba-3* x WT (♀*slsamba* × ♂WT/♀WT × ♂*slsamba*) (Figure 3h,i). When homozygous *slsamba* mutants were used as pollen recipients, the altered fruit shape was maintained, suggesting a persistent effect on fruit morphology, likely resulting from defective male gametogenesis. This is evident in fruits from back-crosses of emasculated *slsamba* flowers (♀*slsamba-3* × ♂WT), which produced a substantial number of seeds, while no seeds were formed when WT plants were used as recipients (♀WT × ♂*slsamba-3*).

Since fruits are derived from ovarian tissues after pollination, we investigated whether the elongated shape in *slsamba* mutants is determined pre-anthesis. A comparison between pistils from *slsamba* and WT at 6 DBA shows that, while the ovary length remains unaffected, mutants exhibited a reduced ovary diameter, resulting in an increased shape index (Figure 3j,k). These results suggest that the *slsamba* mutation alters ovary morphology before anthesis, likely triggering changes in fruit shape. The elongated fruit shape was consistently observed even when *slsamba* plants were used as pollen recipients in reciprocal crosses with WT, highlighting the persistent effect of the mutation on fruit morphology.

The tomato fruit is composed of distinct tissues, including the pericarp (divided into exocarp, mesocarp, and endocarp), the placenta, the septum, and the locular tissue (Mauxion *et al*., 2021). The pericarp represents about two-thirds of the total fruit weight and plays an important role in determining the fruit's quality (Ho, 1996). The development of the tomato pericarp includes an intense phase of cell division closely linked to cell cycle activity, followed by a phase of cell expansion (Faurobert *et al*., 2007). To determine the cellular origin of the observed morphological changes in the ovary and fruit, we investigated the cellular effect of the *slsamba* mutation during pericarp development by performing a time course analysis of pericarp growth from anthesis to 30 DPA (Figure 4a). We observed that the fruits of *slsamba* mutants displayed an increased pericarp thickness compared to the WT (Figure 4b). Additionally, by counting the number of cell layers from the epidermis to the endodermis, we observed an increase in cell layers in *slsamba* fruits, suggesting higher cell division activity (Figure 4c). Furthermore, *slsamba* mutants exhibited smaller cell sizes, although this difference diminished as fruit development progressed (Figure 4d). Notably, cell size alterations in the mesocarp of WT and *slsamba* fruits

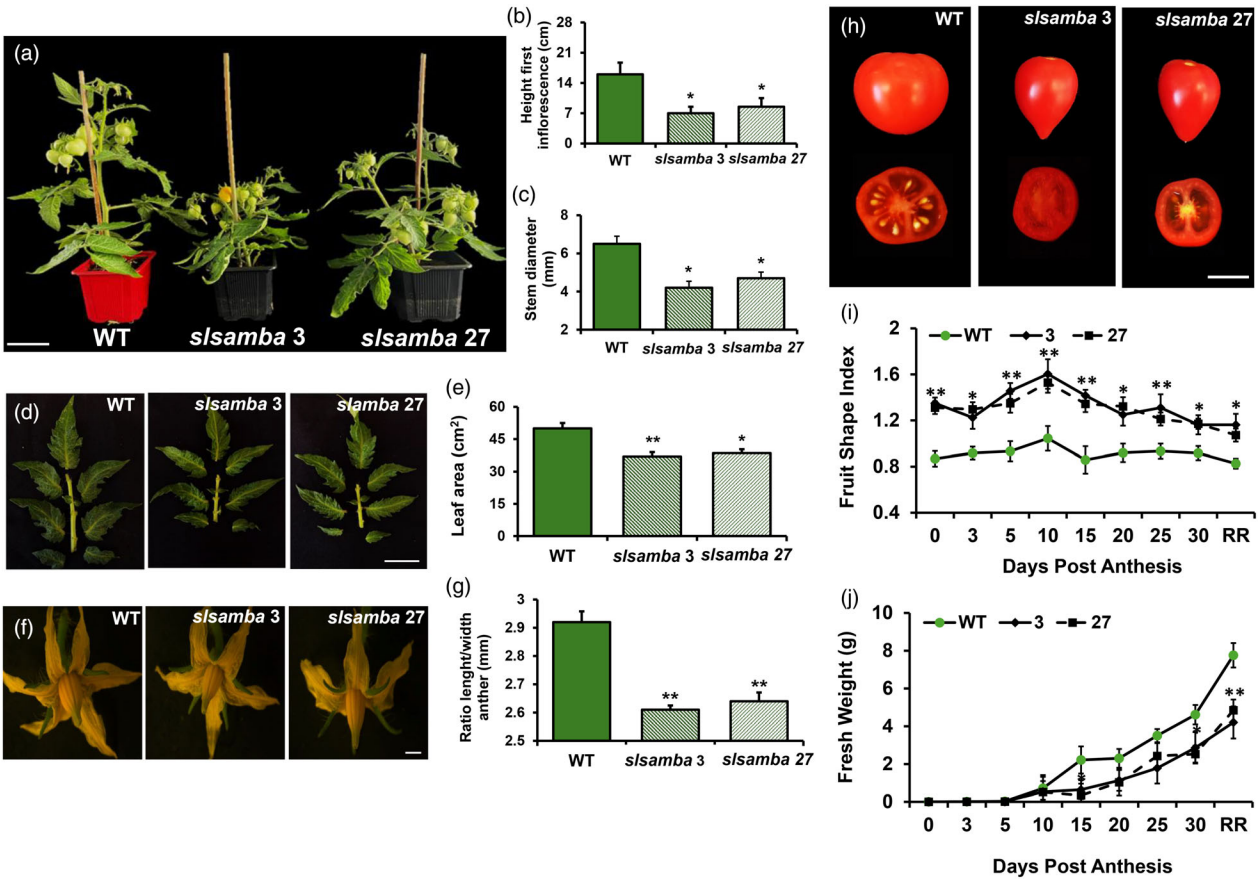

Figure 2 Phenotypic effects of *slsamba* gene editing on tomato plant development. (a) Representative 40-day-old *slsamba* (#3 and #27) and WT plants grown in soil. The edited lines are smaller compared to the WT. (b, c) Height of the first inflorescence and stem diameter of WT and *slsamba* mutants. Data are means ± SEM (n = 12). (d, e) Morphology of the 5th leaf in WT and *slsamba* and total leaflet area of one leaf were measured 1 month after sowing. Data are means ± SEM (n = 21). (f, g) Flowers at anthesis in WT and *slsamba* were observed by stereo microscopy (SMZ 1500 increased 7.5×). *Slsamba* mutants have a reduced average anther length/width ratio at anthesis. Data are means ± SEM (n = 21). (h) Mature fruits of WT and *slsamba* plants. (i) Fruit shape index and (j) weight of the third fruit per inflorescence for WT and slsamba at different stages. Data are means ± SEM (n = 24). Significant differences (ANOVA followed by Dunnett's test) are indicated by asterisks (*P < 0.05 and **P < 0.01).

were more evident at 0 DPA and 10 DPA. We also observed that mesocarp cells in *slsamba* mutant fruits were more irregular in shape than those in WT fruits, with a more elongated appearance. Additionally, mutant fruits showed a 70% increase in cell number compared to WT fruits, indicating a higher cell density within the same area (Figure 4e). Since during fruit development, cell expansion is associated with endoreduplication, we performed flow cytometry analysis on nuclei isolated from the pericarp from 5 DPA to the red ripe stage. Surprisingly, the analysis revealed that ploidy profiles in the *slsamba* mutants were not altered (Figure S6).

Slsamba mutation broadly alters primary and secondary metabolism

We further explored whether the altered fruit phenotype in the *slsamba*-edited plants is associated with or accompanied by changes in their metabolic profiles. Since *SlSAMBA* expression is highest during the early stages of fruit development (Figure 1c), fruit samples were collected at 3, 5, and 8 DPA, and their primary and specialized metabolite contents were analysed by gas chromatography coupled with mass spectrometry (GC–MS) and liquid chromatography coupled with mass spectrometry (LC–MS), respectively. We identified 41 primary metabolites, including 17 amino acids, 13 organic acids, three sugars, two fatty acids, and two sugar alcohols (Table S3). The heat map representing metabolite accumulation in the different genotypes revealed several differences between *slsamba* and WT that collectively contributed to clustering samples in partial least square-discriminant analysis (PLS-DA) (Figure S7). As expected, samples from both *slsamba* lines overlapped and separated from the WT on PLS-DA components 1 and 2, which together explained 40.3% of the total variance. The most important metabolites contributing to this separation (variable importance in projection (VIP) > 1.5) were glucose, aspartic acid, sucrose, oxoglutaric acid, and GABA (Figure S7c).

Given that primary metabolites are major components of fruit quality (Beauvoit *et al.*, 2014), we examined the significant differences in *slsamba* lines compared to WT in more detail (Figure 5a). Except for glucose, soluble sugars were usually at higher levels in the fruits of *slsamba* mutants. This result agrees with the high sucrose demand during the cell division stage of fruit development (Biais *et al.*, 2014; Liu *et al.*, 2007).

The levels of most amino acids also varied significantly between *slsamba* and WT fruits at the time points analyzed (Figure 5a).

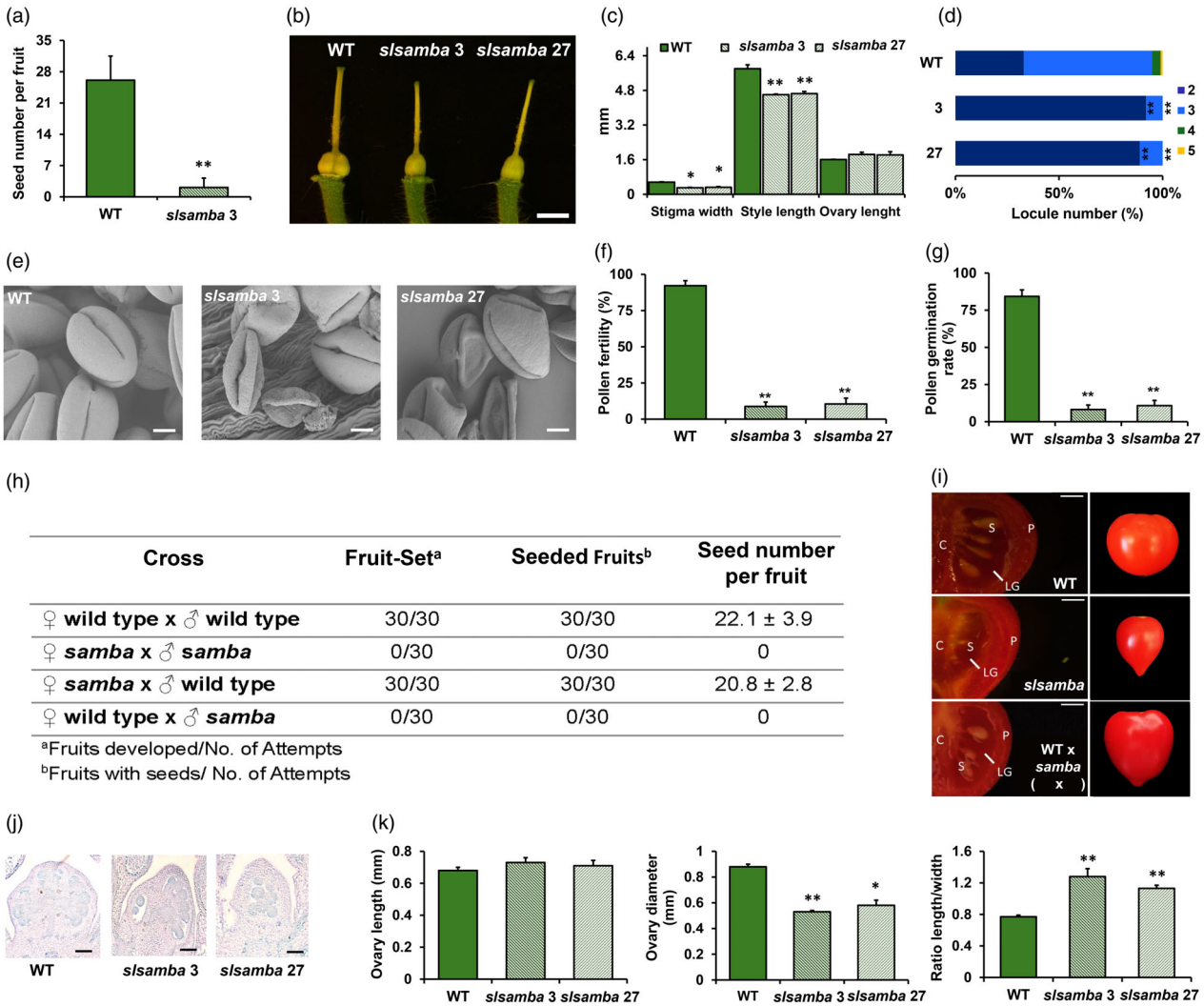

Cross	Fruit-Set[a]	Seeded Fruits[b]	Seed number per fruit
♀ wild type x ♂ wild type	30/30	30/30	22.1 ± 3.9
♀ *samba* x ♂ *samba*	0/30	0/30	0
♀ *samba* x ♂ wild type	30/30	30/30	20.8 ± 2.8
♀ wild type x ♂ *samba*	0/30	0/30	0

[a]Fruits developed/No. of Attempts
[b]Fruits with seeds/ No. of Attempts

Figure 3 Phenotypic effects of the *slsamba* mutation on female and male gametophytes. (a) Seed number per fruit from spontaneous self-pollinations (♀WT × ♂WT/ ♀*slsamba-3* × ♂*slsamba-3*). (b, c) Pistil phenotypes of WT and *slsamba* plants; scale bar = 2 mm. The edited lines have shorter stigma width and style length compared to the WT, but the ovary length is not statistically different. Data are means ± SEM (n = 21). (d) Number of locules in WT and *slsamba* mutants. Locule number quantifications are represented by stacked bar plots (n = 8 plants). (e) Electron micrographs of WT and *slsamba* pollen grains (scale bar = 5 μm). (f, g) Pollen viability [(number of viable pollen grains)/(number of total pollen grains counted × 100)] and pollen germination [(number of germinated pollen grains)/(number of total pollen grains counted × 100)]. Results are expressed as mean values ± SE, considering 10 optical fields randomly selected. (h) Total fruit set and seeded fruits from WT or *slsamba* emasculated flowers crosses (♀WT × ♂WT/♀*slsamba* × ♂*slsamba*) and back-crosses (♀*slsamba* × ♂WT/ ♀WT × ♂*slsamba*). (i) Representative longitudinal sections of WT, *slsamba*, and ♂WT x ♀*slsamba* ripe fruits, where seeds can be observed more frequently in WT and ♂WT x ♀*slsamba* but not in the mutant. C, columella; S, seed; P, pericarp; LG, locular gel; scale bar = 2 mm. (j) Histological analysis of longitudinal sections of ovaries at −6 days before anthesis (DBA) of WT and *slsamba* mutants; Bars = 100 μM. (k) The average ovary diameter, ovary length, and ovary shape index were calculated using ImageJ. Data are means ± SEM (n = 9). Significant differences (ANOVA followed by Dunnett's t test) are shown by asterisks (*P < 0.05 and **P < 0.01).

Alanine, aspartic acid, proline, serine, and threonine were notably elevated in *slsamba* fruits, while GABA, glycine, lysine, methionine, phenylalanine, and branched-chain amino acids (valine, leucine, and isoleucine) were reduced in the mutant compared to the WT. It seems likely that these alterations might, at least partially, be related to the rates of protein synthesis essential for cell division.

Concerning organic acids, the levels of fumaric acid, glycollic acid, oxoglutaric acid, and succinic acid decreased at 8 DPA in *slsamba* mutants, whereas malic acid and quinic acid levels increased compared to the WT. TCA cycle intermediates provide carbon skeletons for the biosynthesis of most amino acids (Galili *et al*., 2016). Additionally, the accumulation of organic acids during the early stages of fruit development is closely related to the supply of substrates that fuel respiration in this climacteric species (Seymour *et al*., 2013).

We also identified 47 specialized metabolites via LC–MS (Figure S8) and quantitative enrichment analysis (Figure S8d) revealed that steroidal glycoalkaloids, alcohols and polyols, flavones, flavonoid glycosides, indolyl carboxylic acids and derivatives, flavans and hydroxycinnamic acids and their derivatives were different between *slsamba* and WT fruits. PLS-DA analysis revealed that the total variability explained was 66.3% (37.9% from component 1 and 28.4% from component 2)

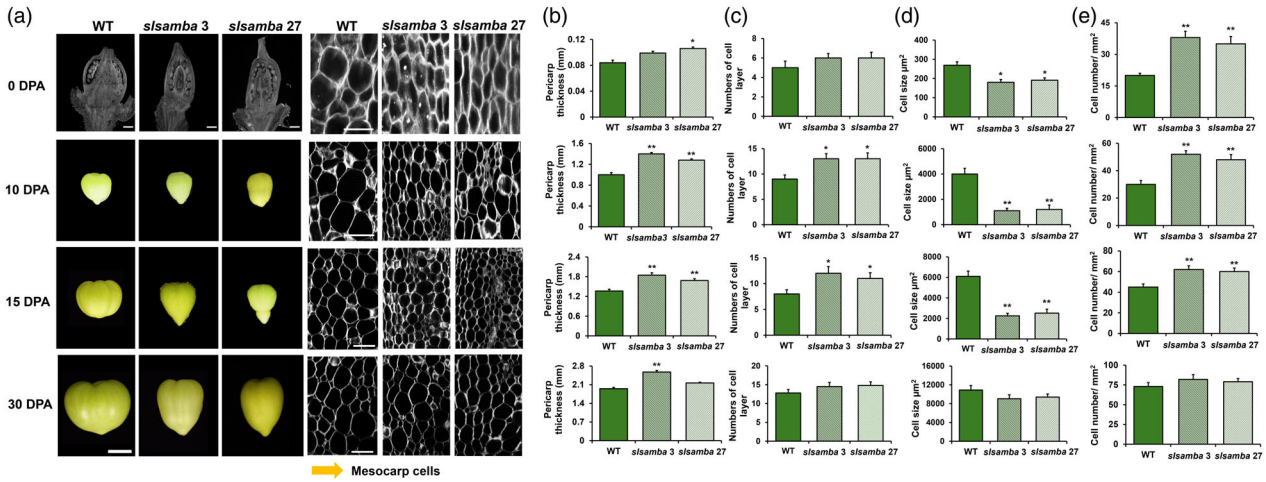

Figure 4 Cell number and cell size alterations in *slsamba* fruits. (a) Morphology of fruits and microscopic observations of wild-type Micro-Tom (WT) and *slsamba* mesocarp cells (#3 and #27) at 0 (Bar = 300 μM), 10 (Bar = 20 μM), 15 (Bar = 20 μM), and 30 days post-anthesis (DPA) (Bar = 200 μM). (b) Pericarp thickness, (c) number of cell layers in the pericarp, (d) average cell size, and (e) cell numbers per area in the mesocarp regions in the WT and *slsamba* mutants. Data are means ± SEM (n = 9). Significant differences (ANOVA followed by Dunnett's t test) are shown by asterisks (*P < 0.05 and **P < 0.01).

(Figure S8a). Metabolite abundance was visualized with a heatmap (Figure S8b) and the 15 with significant changes (ANOVA P < 0.05) are shown in Figure 6. The levels of steroidal glycosides, tryptophan, and caffeoyl glucarate decreased with *slsamba* deletion, while flavone, flavonol, and flavonoid glycosides increased, possibly playing crucial roles in neutralizing reactive oxygen species and modulating responses to pathogens (Chiocchio *et al*., 2023; Frandsen and Narayanasamy, 2018).

To further investigate whether the metabolic differences observed at early fruit development persist, we performed metabolic profiling on red ripe fruits from both *slsamba* mutants and WT plants. *Slsamba* lines still show distinct primary metabolite accumulation patterns compared to the WT (Figure 5b), resulting in a clear separation by PLS-DA analysis (Figure S7e). While some amino acids (e.g. GABA, leucine, isoleucine, and threonine) were present in lower levels in the *slsamba* mutants during early fruit development, their levels were significantly increased in red ripe fruits compared to the WT (Figure S7d). These findings indicate that although fluctuations in metabolism naturally occur during fruit development, the metabolic changes observed in *slsamba* differ from the WT. This might reflect shifts in carbon–nitrogen balance as well as energy metabolism.

Specialized metabolites were also affected in *slsamba* fruits at the ripening stage (Figure 6b). Caffeic acid hexoside, caffeoyl quinic acid, ferulic acid, coumaric acid, kaempferol-3-O-rutinoside, phenylalanine, and cyanidin-3-glucoside were more abundant in *slsamba* mutants compared to the WT. PLS-DA analysis (Figure S8e) and the corresponding heatmap (Figure S8f) confirmed distinct metabolic profiles between genotypes at 52 DPA. Many of the differentially accumulated compounds are derived from the phenylpropanoid pathway, including phenolic acids and flavonoid glycosides.

We also measured the soluble solids content (°Brix) in the red ripe fruits, and the values in *slsamba* were on average 6.3, representing nearly a 20% increase in soluble solids compared to the WT (on average 5.27) (Figure S9). This increase is comparable to the gains achieved by major QTLs associated with improved Brix in tomatoes (Fridman *et al*., 2004; Zhang *et al*., 2024).

Loss of SlSAMBA function leads to cumulative up-regulation of sugar transporter and cell wall modification genes during early tomato fruit development

To examine the effect of *SlSAMBA* disruption at the global transcriptome level, RNA-seq analysis was performed on fruits of *slsamba-3* and WT plants at the same developmental stages as the metabolic profiling. We found 469 differentially expressed genes (DEGs) at 3 DPA, 615 DEGs at 5 DPA, and 4091 DEGs at 8 DPA (adjusted P-value <0.05 and absolute $\log_2$(fold change) > 1.5), representing 3.6%, 3.3%, and 22.8% of the total expressed genes at each time point (Figure S10; Data S3). Several DEGs appeared similarly altered across the three time points, mostly among the down-regulated genes (Figure S10). At both 5 and 8 DPA, the majority of DEGs appeared up-regulated (Figure S10a), and most genes up-regulated at 5 DPA maintained this profile at 8 DPA (Figure S10c). The increase in the number of DEGs over time and the DEGs shared between 5 and 8 DPA suggest that the absence of *SlSAMBA* during the initial stages of fruit development leads to cumulative disturbances in the transcriptional landscape of the tomato fruit.

To shed light on how these transcriptional changes might explain the phenotypes of *slsamba* fruits, we conducted functional enrichment analyses of the DEGs using MapMan4. DEGs were significantly represented in 52 sub-bins belonging to 11 different biological processes, including cell wall organization, protein homeostasis, and solute transport (Figure 7; Data S4). Similar results were obtained from a functional enrichment analysis of Gene Ontology (GO) terms (Data S4).

Several genes in the solute transport category (Figure 7, BIN 24) are involved in sugar transport and were more abundant at 5 and 8 DPA. Upon further examination, we found that eight different sugar transporter gene families were altered in the *slsamba* mutants, totalling 38 DEGs (Data S5). This number corresponds to 46.9% of all described sugar transporters in tomato (Feng

(a)

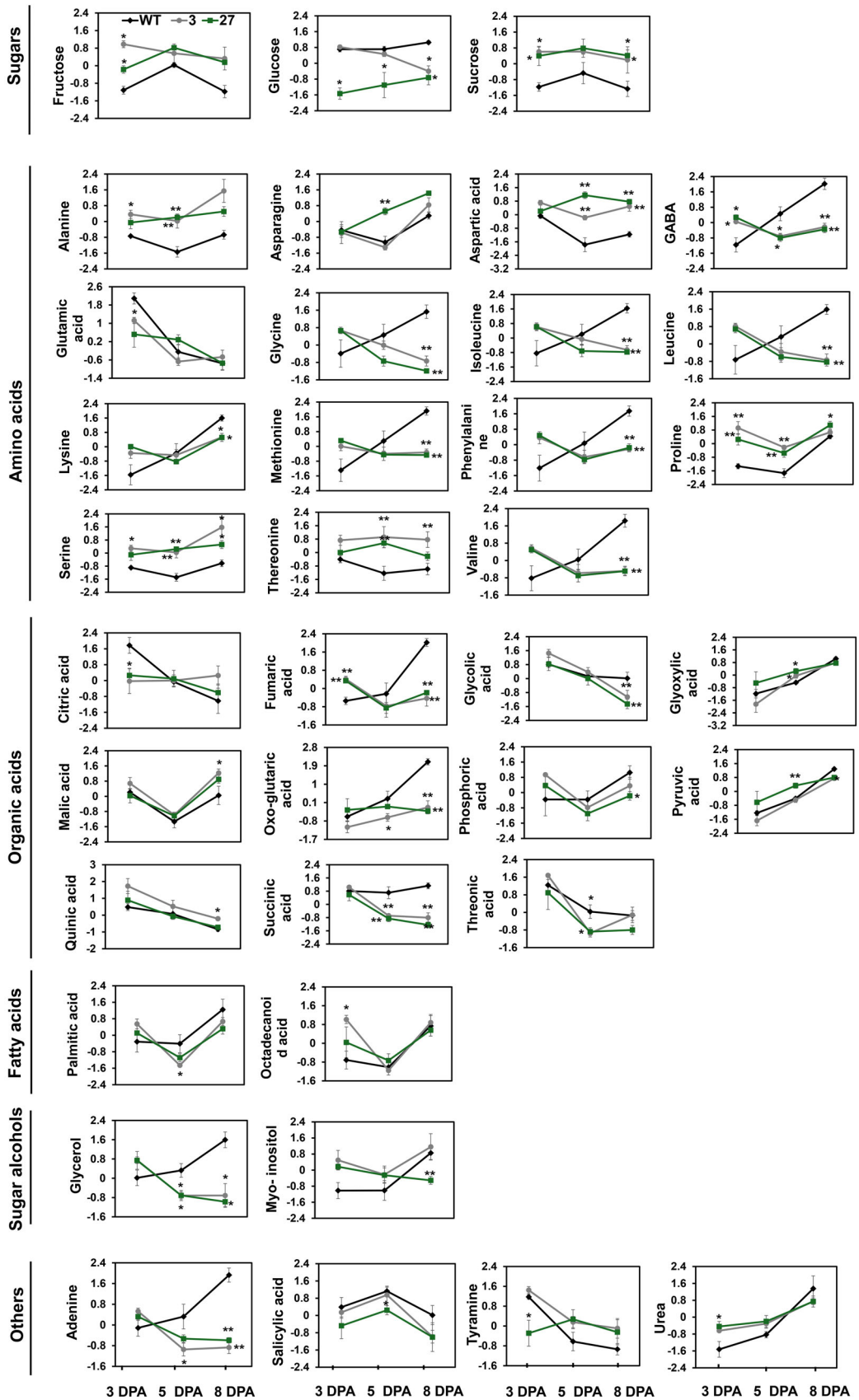
Sugars
WT
3
27
Fructose
Glucose
Sucrose
Amino acids
Alanine
Asparagine
Aspartic acid
GABA
Glutamic acid
Glycine
Isoleucine
Leucine
Lysine
Methionine
Phenylalanine
Proline
Serine
Thereonine
Valine
Organic acids
Citric acid
Fumaric acid
Glycolic acid
Glyoxylic acid
Malic acid
Oxo-glutaric acid
Phosphoric acid
Pyruvic acid
Quinic acid
Succinic acid
Threonic acid
Fatty acids
Palmitic acid
Octadecanoid acid
Sugar alcohols
Glycerol
Myo- inositol
Others
Adenine
Salicylic acid
Tyramine
Urea
3 DPA
5 DPA
8 DPA

Figure 5 Primary metabolites were significantly altered in the fruits of *slsamba* mutants compared to the WT. (a) Relative metabolite quantification was performed by gas chromatography coupled with tandem mass spectrometry (GC–MS/MS) using fruits from individual homozygous plants of lines 3 and 27 and WT plants harvested at early fruit development (3, 5 and 8 days post-anthesis). Metabolites were identified based on receiver operating characteristic (ROC) curves using log and auto-scaling normalized data on the MetaboAnalyst platform 6.0. Data are means ± SD (n = 4–6). Grey and green lines indicate lines 3 and 27, respectively. (b) Primary metabolites were significantly altered in red ripe fruits (52 DPA) of *slsamba* mutants compared to the WT. Data are means ± SD (n = 7). Significant differences (one-way ANOVA, post hoc paired t-test) between the WT and each mutant line are indicated by asterisks (*P < 0.05 and **P < 0.01).

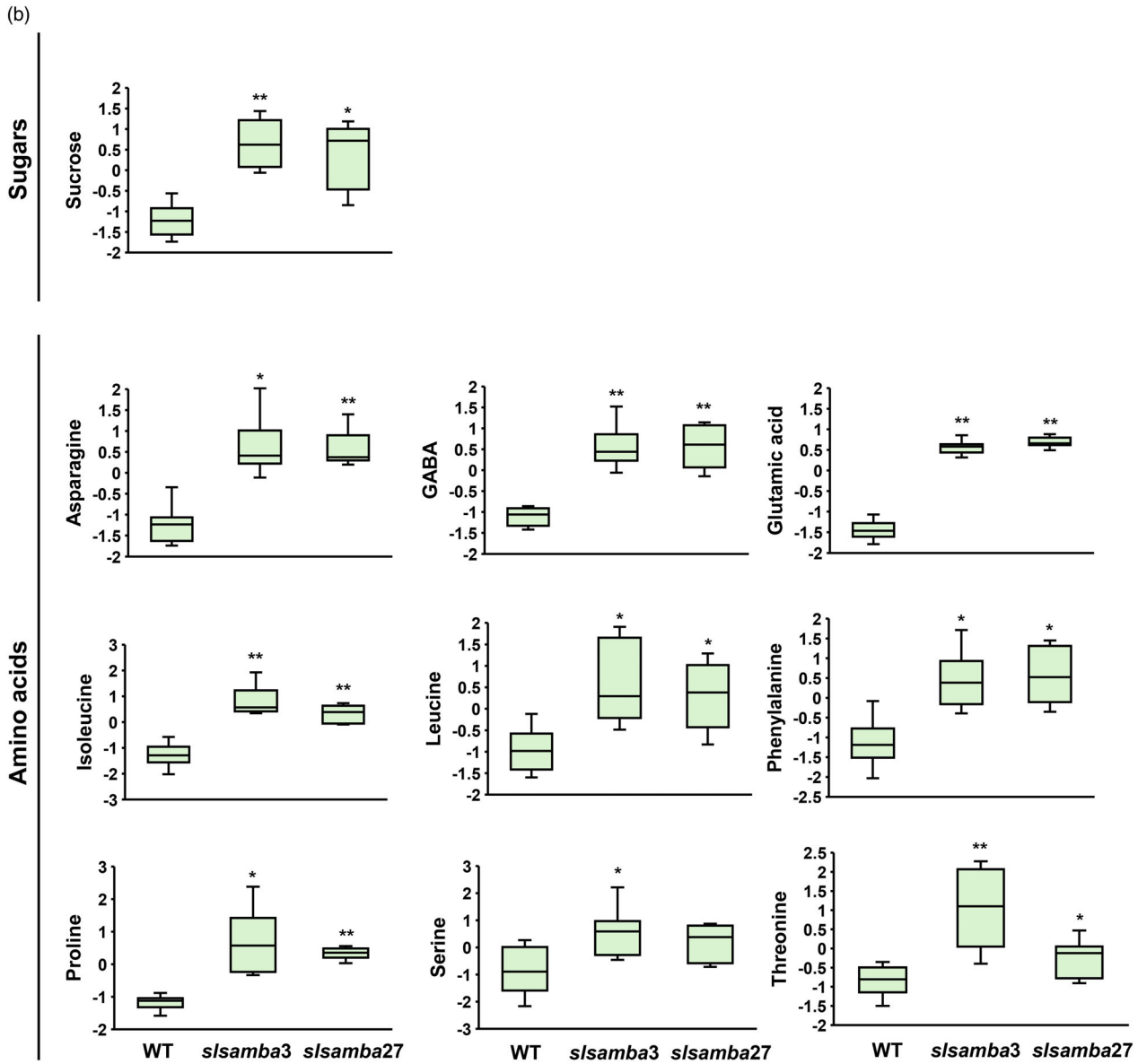

Figure 5 (Continued)

et al., 2015; Reuscher *et al*., 2014). Most of these genes were up-regulated at 8 DPA (29 genes, Figure 8), although 15 were already up-regulated at 5 DPA (Figure 8).

A gene-metabolite correlation analysis with sugar metabolism-related genes revealed an important pattern of expression that may explain the different sugar abundances in *slsamba* fruits (Figure 8). The presence of sucrose metabolism-related genes among the DEGs further consolidates these findings. Notably, at 8 DPA, 13 genes involved in sucrose degradation were up-regulated, including seven beta-fructofuranosidases (invertases), two hexokinases, two fructose kinases, and two sucrose synthases (Data S6). Of these, four beta-fructofuranosidases were already up-regulated at 5 DPA: *Solyc09g010090*, *Solyc10g085360*, *Solyc10g085640*, and *Solyc08g079080* (*SlVI2*). These early changes indicate that alterations in sucrose metabolism begin at the initial stages of fruit development and may

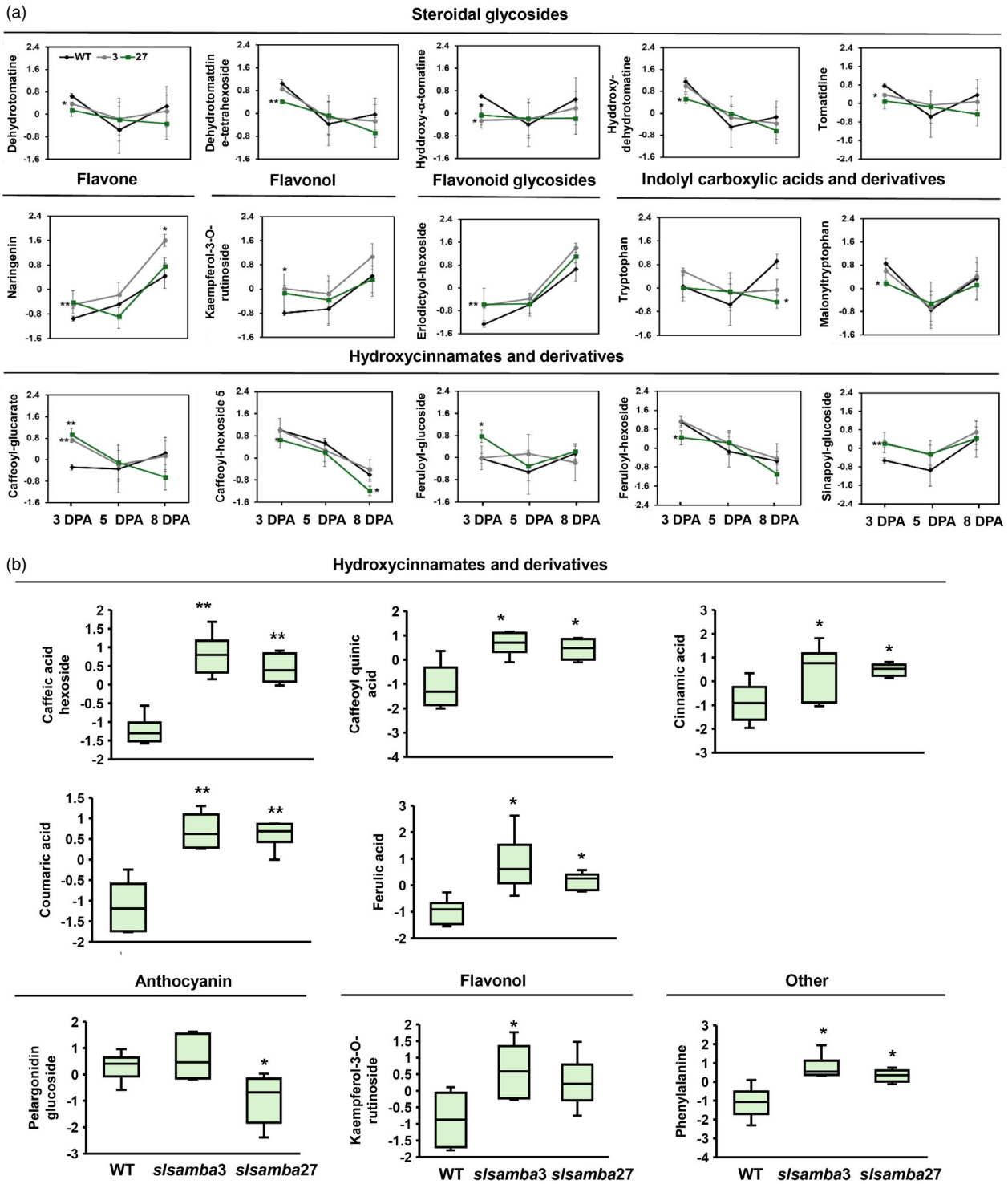

Figure 6 Specialized metabolites were significantly altered in the fruits of *slsamba* mutants compared to the WT. (a) Relative metabolite quantification was performed by liquid chromatography coupled to tandem mass spectrometry (LC–MS/MS) using fruits from individual homozygous plants of lines 3 and 27 and WT plants harvested at early fruit stages (3, 5 and 8 days post-anthesis). Metabolites were identified based on elution time, molecular weight, and MS/MS fragmentation patterns in our databases (Data S2) and were normalized using log and auto-scaling data on the MetaboAnalyst platform 6.0. Data are means ± SD (n = 4–6). Grey and green lines indicate lines 3 and 27, respectively. (b) Quantification of specialized metabolites significantly altered in red ripe fruits (52 DPA) of *slsamba* mutants compared to the WT. Data are means ± SD (n = 6–7). Significant differences (one-way ANOVA, post hoc paired t-test) between the WT and each mutant line are indicated by asterisks (*P < 0.05 and **P < 0.01).

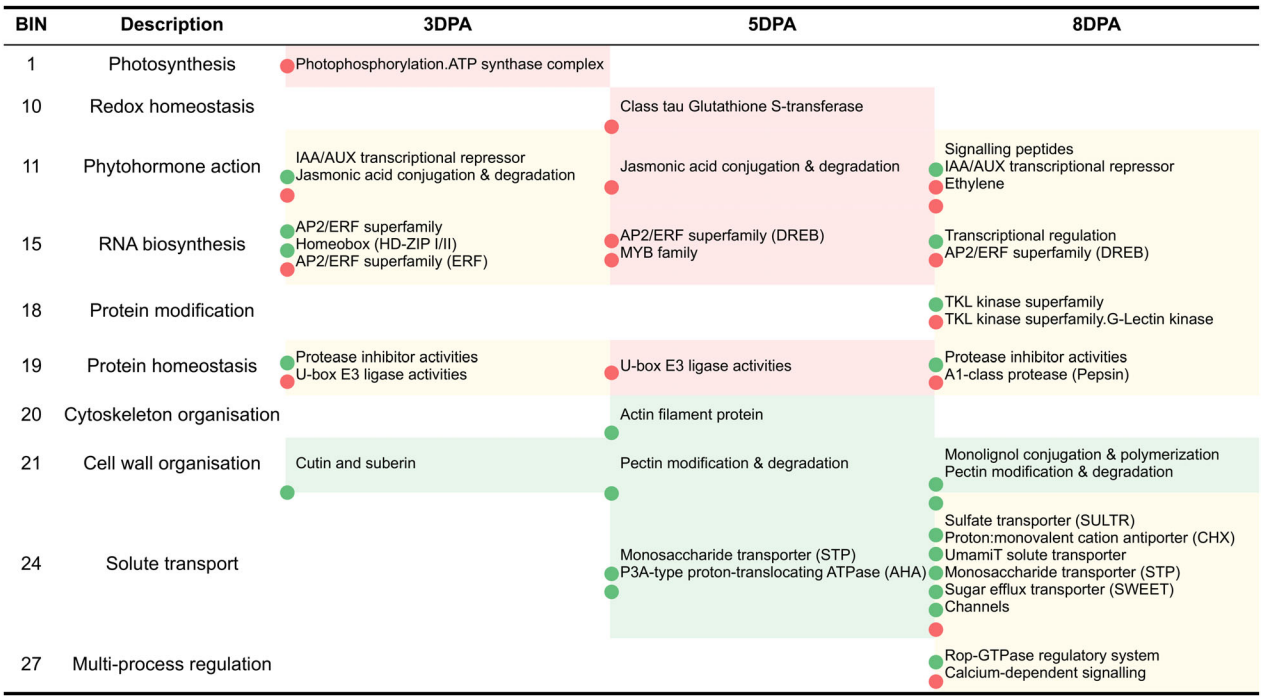

Figure 7 Over-representation analysis of DEGs in MapMan Bins. Enriched top-level MapMan bins are shown on the left, while specific sub-bins are detailed below each time point. Over-representation was determined using the hypergeometric distribution of DEG lists against the background genes (all genes expressed in the analysed samples). Only enrichments with Bonferroni-adjusted *P*-values <0.05 are portrayed. Up- and down-regulated genes were analysed separately. Green boxes correspond to an over-represented bin of up-regulated genes; red boxes correspond to a bin enriched in down-regulated genes; yellow boxes represent bins over-represented in both up- and down-regulated genes. Green circles represent up-regulated bins; red circles represent down-regulated bins. The complete table with the enrichment analysis results is available in Data S3.

contribute to the altered sugar composition observed in the mutants. Our results show that *slsamba-3* fruits exhibit up-regulation of sugar transporters and sucrose degradation enzymes at early developmental stages (5 and 8 DPA), which is unusual for this phase of fruit development (Obiadalla-Ali *et al*., 2004; Ruan and Patrick, 1995).

A Spearman correlation analysis of the expression of these genes with the abundance of different sugars (Figure 8; Data S5) showed that most sugar transporters have a high negative correlation to glucose ($\rho < -0.75$) and a high positive correlation with sucrose ($\rho > 0.75$). Specifically, 23 out of 38 sugar transporter DEGs showed significant correlations with sugar levels ($P < 0.05$). These values indicate that higher expression of these DEGs is associated with lower glucose and higher sucrose content in the fruits, affecting metabolic processes and fruit development.

In the cell wall organization bin (Figure 7, BIN 21), 26 genes were up-regulated at 5 DPA and 138 at 8 DPA, demonstrating a significant and cumulative effect of *SlSAMBA* knockout in cell wall metabolism. Pectin-modifying enzymes were the most enriched in this category at both time points, with 19 up-regulated genes at 5 DPA and 56 at 8 DPA. The expression of pectinesterases and polygalacturonases is linked to pectin degradation, which has a critical role in cell wall remodelling. Their up-regulation at early development stages may affect cell expansion, division, or structural integrity, potentially contributing to the observed fruit shape changes. For instance, the up-regulation of genes encoding pectinesterases and polygalacturonases suggests an acceleration of cell wall loosening processes.

Although the cell division bin did not appear in the MapMan enrichment analysis, several cell cycle-related genes were differentially expressed in the *slsamba-3* fruits. The two APC/C activator protein-encoding genes, *CDC20* (*Solyc08g005420*) and *CCS52* (*Solyc12g056490*) were up-regulated at 8 DPA. Moreover, several cyclins were found among the DEGs. At 3 DPA, four cyclins were up-regulated, including *SlCycB1;2* (*Solyc10g080950*), *SlCycB2;4* (*Solyc04g082430*), *SlCycA3;1* (*Solyc12g088530*), and a cyclin family protein (*Solyc11g030550*). At 8 DPA, four different cyclins were up-regulated: *SlCycA1* (*Solyc11g005090*), *SlCycB2* (*Solyc02g082820*), *SlSDS* (*Solyc04g008070*), and *SlCycU1;1* (*Solyc07g052610*). Additionally, cyclin *SlCycD3* (*Solyc04g078470*) was also up-regulated at both 3 and 8 DPA. The up-regulation of these cyclins, particularly those involved in the G2/M transition, might indicate alterations in the proliferation phase in the mutant.

To validate the RNA-seq data, we selected 10 genes involved in key metabolic and regulatory pathways that showed differences in the *slsamba* mutant: tomatidine biosynthesis (16alpha,22,26-Trihydroxycholesterol, Solyc10g018190), naringenin biosynthesis (*Chalcone synthase SlCHS*, Solyc01g090600; *Chalcone-flavone isomerase SlCHI*, Solyc05g010310), sugar metabolism (*Sucrose Synthase SlSUS*, Solyc03g098290; *Sucrose Phosphate Synthase SlSPS*, Solyc08g042000; *Invertase 6 SlINV6*, Solyc10g0832900) and *transport (Sugars Will Eventually Be Exported Transporter 5a SWEET5a*, Solyc03g114200); and cell cycle regulation (*Cyclin A1 SlCycA1*, Solyc11g005090, *Cyclin D3.3 SlCycD3.3*, Solyc04g078470; *Cell Cycle Switch Protein 52B SlCCS52B*, Solyc12g056490) (Figure S11). These genes were

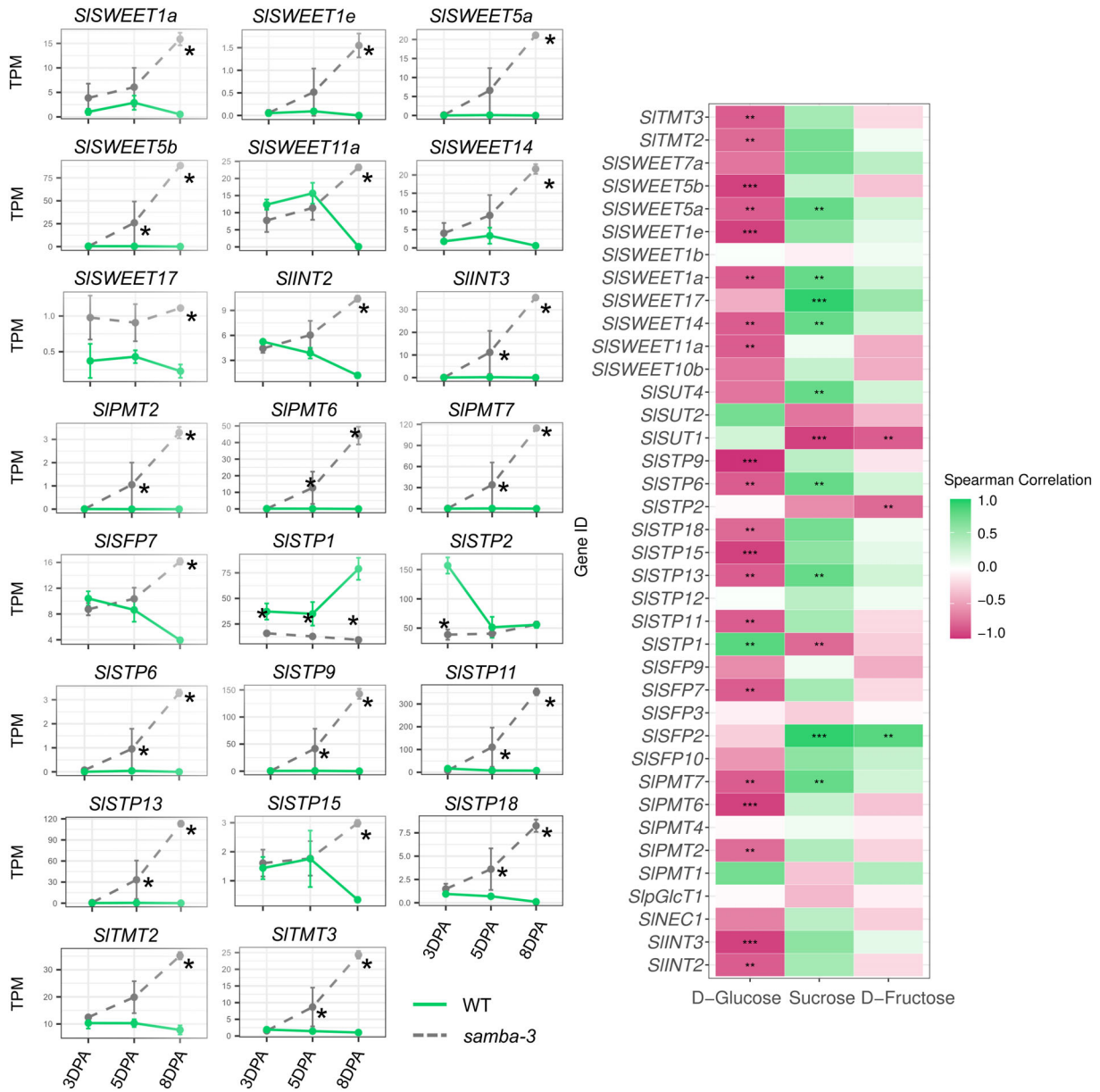

Figure 8 Expression profiles of sugar transporters and their correlation with different sugars. Expression profiles of sugar transporters significantly correlated with different sugars (|ρ| > 0.75). Expression values correspond to normalized TPM values. * = Time point with significant differential expression (adjusted *P*-value <0.05). The heatmap shows Spearman correlation values (ρ) above 0.75 and below −0.75 marked by '**', while values above 0.9 and below −0.9 are marked by '***'.

analyzed using qRT-PCR from *slsamba-3* and WT at 5- and 8 DPA. Additionally, we included RNA samples from the red ripe fruits (52 DPA).

The qRT-PCR results confirmed the expression patterns seen in the RNA-seq data, validating the findings from the earlier stages of fruit development. Overall, the major trends observed in early stages [e.g. genes involved in sugar metabolism that were up-regulated (*SUS*, *SPS*, and *SWEET5a*) or down-regulated (*INV6*) in *slsamba*] remained largely consistent at the red ripe stage. Notably, *CHS* and *CHI* showed even higher expression levels compared to WT at 52 DPA. These data suggest a sustained alteration in sugar accumulation and transport and secondary metabolism in *slsamba*, confirmed by the metabolite levels. As expected, the expression of cell cycle genes decreased as the tissue aged. Both genotypes showed very low expression for *CycA1*, *CycD3.3*, and *CCS52B* at 52 DPA.

DEGs in *slsamba* loss-of-function plants show enrichment in specific transcription factor (TF)-binding sites

Given the pronounced and cumulative effects of *SlSAMBA* loss of function on gene expression in developing tomato fruit, we investigated whether the *samba* DEGs contain enriched TF binding sites in their regulatory regions. To explore this, we performed a TF-binding site enrichment analysis in the 2-kb upstream sequence of the translation start site of the *slsamba* DEGs, comparing them to all genes expressed at each respective developmental stage sampled (Data S6).

Table 1 Enrichment of TF-binding sites at timepoints 3 DPA and 5 DPA

TF Family	# Motifs	# Expressed TFs	π-values
3 DPA Up-regulated			
bHLH	24	27	[1.30–0.74]
Homeodomain	5	16	[0.75–0.70]
Sox	1	7	[0.31–0.31]
bZIP	1	6	[0.75–0.75]
EIN3	1	5	[1.10–1.10]
3 DPA Down-regulated			
AP2	104	40	[6.29–0.60]
WRKY	96	31	[6.30–0.94]
bHLH	30	29	[1.92–0.61]
NAC/NAM	29	13	[5.42–0.28]
Myb/SANT	23	17	[1.78–0.36]
5 DPA Up-regulated			
None			
5 DPA Down-regulated			
WRKY	93	37	[11.42–0.54]
AP2	88	62	[8.14–0.64]
Sox,WRKY	17	7	[4.67–0.84]
NAC/NAM	11	16	[5.27–0.56]
E2F	10	4	[1.96–0.71]

The top five TF families with the highest number of enriched motifs at time points 3 DPA and 5 DPA. Expressed TFs are transcription factors known to bind to at least one of the enriched binding sites, which are themselves expressed at the respective time point. The p-value range indicates the significance of the motif enrichment within each family, where higher values are more significant (a combination of adjusted *P*-value and enrichment fold; see methods).

Interestingly, within the upregulated DEGs at 3 DPA, our analysis revealed a clear enrichment for motifs of bHLH and homeobox TFs (Table 1). This finding aligns with the GO analysis of the DEGs at 3 DPA, though due to the broad functional roles of bHLH TFs in diverse processes (Gao and Dubos, 2024; Hao *et al*., 2021), specificity is challenging. Notably, Arabidopsis orthologs of these bHLH and homeobox TFs (specifically from the Glabra subgroup) are known to synergistically regulate metabolic pathways (Nguyen *et al*., 2023). Conversely, among the down-regulated DEGs at 3 DPA, motifs for WRKY and AP2 TFs were enriched, corresponding with the GO analysis of DEGs in which defence categories are enriched (Data S4).

At later time points, enrichment is either absent or far less pronounced. Only within the downregulated DEGs at 5 DPA, there is still enrichment for motifs of WRKY and AP2 TFs (Table 1). No enrichment was observed in the upregulated DEGs at 5 DPA, while at 8 DPA (in both up- and downregulated DEGs), different TF classes were enriched (Data S7), suggesting that the *SlSAMBA* knockout signal is dispersing and that secondary effects are predominant. This result supports the previous indication that loss of *SlSAMBA* during the early stages of fruit development leads to cumulative disturbances in the transcriptional landscape of the tomato fruit at later stages.

Discussion

Although the APC/C plays a crucial regulatory role in the eukaryotic cell cycle (Alfieri *et al*., 2016), knowledge of its function in plants lags behind that of mammals and yeast. Here, we identified *SlSAMBA* as a homologue of *SAMBA* in Arabidopsis, sharing strong similarities with tobacco and exhibiting conservation of key motifs in its protein sequence (Figure 1). The *SlSAMBA* gene is highly expressed during early flower and fruit development, particularly in floral buds and in fruits up to 10 DPA, a stage associated with intense cell division, supporting its potential role in cell division regulation (Quinet *et al*., 2019). In the later stages of flower development, *SlSAMBA* expression decreases and becomes spatially restricted, as observed at anthesis, where it is limited to the stigma and ovary. This pattern differed slightly from that observed in Arabidopsis *SAMBA (AtSAMBA)*, which was highly expressed during embryogenesis, gradually decreasing during seedling germination, and becoming restricted to the hypocotyl after 8 DAS (Eloy *et al*., 2012). In later stages of flower development, *AtSAMBA* was confined to the pollen grains, a pattern similar to that observed for *SlSAMBA* in tomato. However, unlike in tomato, *SAMBA* was not observed in Arabidopsis female gametophyte, suggesting an additional function for *SlSAMBA* during female gametophyte development specific to the species, as highlighted by the phenotypic alterations observed in *slsamba*.

Stable expression of the SlSAMBA-TurboID fusion in tomato roots revealed seven proteins with more than a 4-fold (log2) enrichment, indicating strong proximity or interaction with SlSAMBA. Among the identified proteins, we found homologues of APC3b and APC6, well-known APC/C subunits, as well as two Arabidopsis homologues of NAP1-RELATED PROTEIN 2 (NRP2), which are also involved in cell cycle control (Wang *et al*., 2020). These findings support the hypothesis that SlSAMBA is a member of the APC/C complex, as previously reported for Arabidopsis and maize (Eloy *et al*., 2012; Gong *et al*., 2022).

Using the CRISPR/Cas9 editing system, we generated *slsamba* mutant lines with pleiotropic effects, uncovering new roles for SAMBA that were not previously described. The knockout lines displayed a dwarf phenotype characterized by smaller vegetative and reproductive structures. Compared to WT plants, *slsamba* mutants exhibit reduced overall stature, stem diameter, and leaf area. Similar vegetative phenotypes were observed in maize CRISPR-edited *samba* mutants in which reduced plant stature highlighted the conserved role of SAMBA in regulating plant size (Gong *et al*., 2022). The *slsamba* mutants also exhibited smaller flowers, thinner anthers, and impaired pollen development, which could negatively impact reproductive success and seed yield. Similarly, disruptions in the APC/C complex in Arabidopsis have been shown to impair gamete viability or embryo formation, ultimately leading to reduced seed production (Capron *et al*., 2003; Kwee and Sundaresan, 2003; Pérez-Pérez *et al*., 2008; Eloy *et al*., 2011 Wang *et al*., 2012, Wang and Ruan, 2013; Guo *et al*., 2018). This impact on fertility is due to impaired cell cycle progression in reproductive structures (Bolaños-Villegas *et al*., 2018; Sprunck, 2020). Despite the many differences observed in vegetative and reproductive development, no noticeable variations in fruit ripening progression were observed between the *slsamba* and WT plants under greenhouse conditions.

The phenotypic outcomes of *SAMBA* loss-of-function mutants highlight differences in the roles of SAMBA proteins across species. In *Arabidopsis*, loss of *AtSAMBA* leads to larger organs, suggesting that AtSAMBA functions as a negative regulator of growth (Eloy *et al*., 2012). In contrast, loss of *ZmSAMBA* in maize (Gong *et al*., 2022) and *SlSAMBA* in tomato results in reduced organ size, indicating that SAMBA acts as a positive regulator of

growth in these species. This functional divergence is particularly intriguing given the evolutionary relationships among these species, and we propose two possible explanations for this difference. (1) The role of SAMBA in maize may reflect its ancestral function, which has been retained in tomato but altered in *Arabidopsis* through evolutionary adaptation. Although *Arabidopsis* and tomato are both eudicots, they belong to distinct phylogenetic groups, Rosids and Asterids, respectively. (2) Maize and tomato may have independently evolved similar regulatory mechanisms involving SAMBA, leading to comparable phenotypes. Differences in protein–protein interaction networks may contribute to the observed functional shifts. At the structural level, despite attempts to predict the 3D structures of SAMBA proteins, current computational models provide low-confidence predictions, limiting direct structural comparisons. Further experimental studies, such as X-ray crystallography or cryo-electron microscopy, will be required to resolve their structures and clarify how sequence differences translate into functional divergence. Nevertheless, sequence analysis reveals that the central 'RKDEAxxxLK' motif is conserved in all three species, suggesting a core function. However, both SlSAMBA and ZmSAMBA possess longer C-terminal regions with an increased number of lysine (Lys) residues compared to AtSAMBA (5 and 4 vs. 3, respectively). These lysine-rich regions could influence protein–protein interactions or post-translational modifications, such as ubiquitination or acetylation, which might contribute to functional divergence. Given that ubiquitination plays a crucial role in APC/C activity, alterations in these regions could impact protein stability and function differently across species.

Elongated fruit shape is often associated with imbalances in cell proliferation and expansion across the pericarp layers (Xiao *et al*., 2008; Wu *et al*., 2018). Our fruit cytological analysis revealed increased cell division supported by a greater number of cell layers in the pericarp of *slsamba* plants compared to WT. Additionally, the cell size in the mesocarp was significantly smaller than in WT, resulting in an increased cell number within the same analyzed area. These features likely contribute to the observed phenotype, highlighting the critical role of SAMBA in regulating the cell division cycle.

Metabolomic analysis of *slsamba* mutants further highlights significant changes in metabolites, particularly amino acids, suggesting a shift in nitrogen distribution potentially regulated by SlSAMBA. This modulation, especially in the key nitrogen carrier glutamine, impacts both fruit growth and flavour characteristics (Beauvoit *et al*., 2014). In addition, *slsamba* fruits have higher sucrose content, and it remains to be elucidated whether this is due to increased fruit sink activity, altered futile cycles involving sucrose synthesis and degradation, or a combination of both. RNA-seq data indicate that the *slsamba* mutant shows an early up-regulation of sugar transporter genes and sucrose-degrading enzymes (sucrose synthases, fructokinase, hexokinase, and invertases), suggesting altered sugar transport and accumulation at early developmental stages. Sugars serve as both metabolites and signalling molecules in plant development, potentially influencing the expression of cell cycle genes (Chen *et al*., 2021; Smeekens *et al*., 2010). In cultivated tomato varieties, fruits typically accumulate hexoses, with phloem unloading during early development occurring primarily through the symplastic pathway (Ruan and Patrick, 1995; Wang and Ruan, 2013). This symplastic unloading involves the direct transfer of sugars between cells via plasmodesmata, bypassing the need for transporter proteins (Patrick, 1997; Braun, 2022).

As the fruit matures, there is a developmental shift to apoplastic unloading, which requires the activity of invertases to hydrolyze sucrose and hexose transporters to facilitate sugar uptake into cells (Ruan and Patrick, 1995; Wang and Ruan, 2013; Julius *et al*., 2017). An early shift to apoplastic unloading would typically result in higher hexose levels (Dali *et al*., 1992; Yelle *et al*., 1988), which is not the case for *slsamba* fruits. Despite the up-regulation of invertase genes in *slsamba* fruits, the actual enzyme activity might be reduced or inhibited, leading to the observed sugar profile. A recent study on metabolite variation during tomato fruit development (cv Moneymaker) revealed that not always a direct correlation between a metabolite and the transcripts or proteins related to its specific pathway can be found, indicating complex regulations involving coordinated changes at these different levels (Moing *et al*., 2023).

Sun *et al*. (2022) reported that the differential expression of sugar transporters explains whether a tomato fruit accumulates hexoses or sucrose. By analyzing both sucrose- and hexose-accumulating cherry tomatoes, the authors observed distinct patterns in enzyme activities and transporter expression. In hexose-accumulating tomatoes, high activities of acid invertase, sucrose phosphate synthase (SPS), sucrose synthase (SS), and specific transporters from the SUT and SWEET families are prominent. For sucrose-accumulating fruits, the combination of SPS, SS, and other SUT and SWEET transporters was observed. In our dataset, two *SPS* and two *SS* genes were up-regulated at 5 and 8 DPA, while *SlSUT1* was down-regulated at 3 DPA, *SlSUT2* was down-regulated at 8 DPA, and *SlSUT4* was up-regulated at 8 DPA. Regarding SWEET transporters, the activity of SlSWEET1b, SlSWEET5b, SlSWEET11b, SlSWEET7a, and SlSWEET14 is important for sucrose accumulation (Sun *et al*., 2022). Of these, only *SlSWEET1b* was not up-regulated in *slsamba* fruits. None of the glucose-accumulating-related SWEET transporters mentioned by Sun *et al*. (2022) were differentially expressed in *slsamba* fruits. This pattern supports the idea that the up-regulation of specific sugar transporters and metabolic enzymes in *slsamba* fruits contributes to sucrose rather than hexose accumulation in a complex manner.

Elevated intracellular sucrose may serve as a signal influencing gene expression related to the cell cycle (Rawat and Laxmi, 2024), as evidenced by the up-regulation of cyclins such as *SlCycD3* (Solyc04g078470), potentially enhancing cell proliferation activity in early fruit development (Rawat and Laxmi, 2024; Riou-Khamlichi *et al*., 2000). In Arabidopsis, *CYCD3;1* expression is induced by sucrose (Riou-Khamlichi *et al*., 2000) and sucrose-starved cells exhibit a decline in CYCD3;1 activity, leading to its subsequent degradation via the proteasome-dependent pathway, resulting in hypophosphorylation of RBR1 and arrest at the G1/S transition (Hirano *et al*., 2008, 2011; Menges *et al*., 2006). In our study, several other cell cycle-related genes, including cyclins involved in the G2/M transition (e.g. SlCycB1;2, SlCycB2;4, SlCycA3;1), were up-regulated in *slsamba* fruits. Furthermore, the differential expression of Kip-related proteins (KRPs), which are inhibitors of cyclin-dependent kinases (CDKs), indicates complex regulation of the cell cycle machinery in response to sugar signals (Wang and Ruan, 2013). The up-regulation of some KRPs and the down-regulation of others in *slsamba* fruits may represent a balance between promoting and restraining cell division.

Finally, our TF-binding site enrichment analysis suggests that there may indeed exist a specific TF target for SlSAMBA, with two possible scenarios (or a combination thereof). First, SlSAMBA

could target an activator-bHLH TF (eventually acting synergistically with a homeobox TF), which in the *slsamba* edited line would be overaccumulating, leading to the up-regulated DEGs at 3 DPA. Second, SlSAMBA would target a repressor TF (which could be either a WRKY and/or an AP2-ERF), which in the *slsamba* edited line would be overaccumulating and leading to the downregulated DEGs at 3 DPA. These findings provide an exciting avenue for future research on the molecular mechanisms by which SlSAMBA modulates fruit development and quality.

In conclusion, our findings demonstrate that SlSAMBA influences sugar transport and metabolism, with changes in intracellular sugar concentrations that are a key determinant of taste and economic value (Zhang *et al*., 2024). Furthermore, the higher sugar levels potentially act as signals to regulate cell cycle gene expression. This link highlights the dual role of sugars as both nutrients and signalling molecules in plant development (Chen *et al*., 2021; Smeekens *et al*., 2010). In addition to changes in sugar metabolism, our metabolomic analysis at the ripe red fruit stage revealed that *slsamba* fruits accumulated higher levels of phenolic compounds, including caffeic acid derivatives, ferulic acid, and flavonoid glycosides such as kaempferol-3-O-rutinoside. These compounds are known for their antioxidant properties, suggesting that *slsamba* fruits have both enhanced sugar content and an improved antioxidant profile. Further studies on enzyme activities, sugar and phenylpropanoid signalling pathways, and their impact on cell cycle regulators will provide deeper insights into SlSAMBA's role in fruit development. Understanding how SlSAMBA disruption leads to coordinated changes in sugar metabolism, specialized metabolite biosynthesis, cell proliferation, and organ size could uncover new aspects of fruit growth regulation and the interplay between metabolic and developmental processes.

Materials and methods

Sequence alignment and chromosome location

The *S. lycopersicum* SAMBA protein sequence was downloaded from the Genome Database of Solanaceae (http://solgenomics.net/), and the reported SAMBA proteins in *Arabidopsis thaliana*, *Oryza sativa*, *Sorghum bicolour*, *Vitis vinifera*, *Ricinus communis*, *Populus trichocarpa*, and *Picea sitchensis* were acquired from NCBI. The protein sequence alignment was performed using Clustal X version 2.1 with default parameters (Thompson *et al*., 1997). The tomato *SAMBA* gene was mapped on a chromosome in accordance with the whole genome of this species. The chromosomal location of the identified *SlSAMBA* gene was extracted from the general feature format (GFF) file provided.

Plant material and growth conditions

Seeds of *S. lycopersicum* (tomato) cv. Micro-Tom were surface sterilized with commercial bleach (containing an average of 2%–2.5% active chlorine) and germinated in half-strength MS medium (Murashige and Skoog; Sigma-Aldrich, St. Louis, MO) supplemented with 30 $mg.L^{-1}$ sucrose and 1% agar, pH 5.8. Seeds were incubated at 25 °C under long-day conditions (16 h light (45 μmol $photons.m^{-2}.s^{-1}$ PAR irradiance)/8 h dark). In greenhouse conditions, plants were cultivated with a photoperiod of 16 h/8 h with a mean temperature of 24 °C during the day and a mean temperature of 18 °C during the night. The humidity was around 55% all day, and plants were subjected to daily watering.

Vector construction and plant transformation

Solanum lycopersicum (tomato) cv. Micro-Tom was edited using the CRISPR/Cas9 system to produce *slsamba* mutants. Tomato transformation, CRISPR/Cas9 vector, and primers are described in Table S4. T0 generations of the mutants were backcrossed to wild-type (WT) once or twice to separate alleles and select against Cas9. Mutations were confirmed by Sanger sequencing. The Cas9-free homozygous mutants were obtained in the F2 or F3 generations and used for further analysis.

For the *SlSAMBA* promoter analysis, a 1600 bp genomic fragment (upstream of the ATG start codon) containing the putative promoter region was amplified from the genomic DNA of Micro-Tom tomato plants, cloned into the pDONR221 vector (Invitrogen), and subcloned into the GUS::GFP-containing binary vector pKGWFS7. Micro-Tom transgenic plants were transformed using *Agrobacterium tumefaciens* strain GV3101 as described by Pino *et al*. (2010). Five independent antibiotic-resistant transgenic lines were selected by PCR and were subsequently examined for expression levels.

Subcellular localization of the SlSAMBA protein

Transient expression in *N. benthamiana* leaves via agroinfiltration was performed as described by Zhang *et al*. (2020). *Agrobacterium tumefaciens* strain harbouring the N-terminal GFP fusion vector was grown in LB medium in the presence of antibiotics. The agrobacteria culture was pelleted and resuspended in the infiltration medium (¼MS pH 6.0, 1% sucrose, 100 μM acetosyringone, 0.005% (v/v) silwet L-77) adjusted to an OD_{600} of 0.5. agrobacteria suspension was infiltrated into the abaxial side of the tobacco leaves using a needleless syringe. Images were captured by confocal laser scanning microscopy (Leica TCSSP5 AOBS, Wetzla, Germany). Excitation and emission wavelengths for GFP were 488 nm and 505–530 nm, respectively. The subcellular localization was predicted by using the online tools CELLO v.2.5 (http://cello.life.nctu.edu.tw/) and WoLF PSORT (https://wolfpsort.hgc.jp/). Transmembrane prediction was carried out with HMMTOP software.

RNA extraction and gene expression analysis

Total RNA was isolated from the leaf tissues of tomato cv. Micro-Tom using TRIzol (ThermoFisher, USA), according to the manufacturer's instructions. RNA was quantified using a NanoDrop 2000 spectrophotometer (Thermo Scientific, USA), and its integrity was checked by electrophoresis. To eliminate the residual genomic DNA present in the preparation, the RNA was treated by RNAse-free DNase I according to the manufacturer's instructions (Promega, USA).

The cDNA was synthesized from 1 μg of total RNA using the SuperScript™ III First-Strand Synthesis System, according to the manufacturer's protocol (ThermoFisher, USA). Transgene expression was analyzed by qRT-PCR on an ABI 7500 qPCR thermocycler (Applied Biosystems, USA) using the Platinum SYBR Green Supermix (Invitrogen, USA). Three biological replicates and three technical replicates for each reaction were analyzed. The reaction was initiated at 95 °C for 10 min and followed by 40 amplification cycles of 95 °C for 15 s, 60 °C for 30 s, and 72 °C for 30 s. The target was the *SlSAMBA* (Table S4) and *Slβ-ACTIN* was used as a reference gene, following previous works (Ferreira e Silva *et al*., 2014) (Table S4). The comparative ΔΔCt method was used to calculate relative expression levels in real-time qPCR data (Livak and Schmittgen, 2001). Changes in gene expression

related to sugar synthesis, flavone synthesis, and the cell cycle were also characterized by qRT-PCR using the primers listed in Table S4.

Histochemical GUS assay

Flowers at anthesis and fruits at 10, 15, and 30 DPA and red ripe (RR) fruit from pSlSAMBA::GUS::GFP lines were harvested. Samples were incubated in 50 mM sodium phosphate buffer (pH 7.0) containing 0.9 mM 5-bromo-4-chloro-3-indolyl-beta-D-glucuronide (X-Gluc), 10 mM EDTA, and 0.1% (v/v) Triton X-100 at 37 °C for 2 h for GUS staining. Subsequently, the stained samples were treated with 70% ethanol at 37 °C for 2 days to remove chlorophyll. Images were acquired using the Axio Zoom V16 fluorescence microscope (Zeiss, Germany).

Turbo ID-catalysed proximity labelling

TurboID-mediated proximity labelling involved transformed tomato hairy root cultivation with *Agrobacterium rhizogenes*, sample preparation for mass spectrometry (MS), immunoblot analysis, LC–MS/MS analysis, and MS data analysis, which were all carried out essentially as described (Gryffroy *et al*., 2023a, 2023b).

Yeast two-hybrid assays

The full-length coding sequences (CDS) of *SlAPC10* (*Solyc02g062680*), *SlSAMBA* (*Solyc08g076580.2*), and *SlCDC27B* (*Solyc03g0203431*) were cloned into the pGADT7 and pGBT9 Gateway™ vectors (Cuéllar *et al*., 2013). All CDS were cloned in both vectors. The pGADT7 vector contains the activation domain (AD) of the GAL4 transcriptional activator, while pGBT9 includes the GAL4 DNA-binding domain (BD). The destination vectors were co-transformed into the *Saccharomyces cerevisiae* PJ69-4A strain using the Frozen-EZ Yeast Transformation II Kit (Zymo Research, California, USA). Transformants were selected on SD medium (Takara Bio, Shigo, Japan) lacking leucine and tryptophan (SD -Leu -Trp). Three individual colonies were chosen, grown overnight in liquid culture at 30 °C under 250 rpm agitation, and sequentially diluted (10- to 100-fold). The dilutions were dropped on both control (SD -Leu -Trp) and selective media lacking leucine, tryptophan, and histidine (SD -Leu -Trp -His). Plates were incubated at 30 °C for 3 days.

Phenotypic analyzes

To evaluate morphological diversity among the *slsamba* and wild-type (WT) plants, the height of the first inflorescence and stem diameter were measured in 40-day-old CRISPR-Cas mutants (T2) and WT plants (12 biological replicates (one plant each) per genotype). The morphology of the 5th leaf (21 biological replicates (single leaves) per genotype) and total leaflet area were measured 1 month after sowing. Flowers at anthesis (21 biological replicates (flowers) per genotype) were observed by stereo microscopy (SMZ 1500 increased 7.5×). The length and width areas were quantified using ImageJ (https://imagej.nih.gov/ij/).

Pollen Quantification and Viability

Pollen fertility was determined by counting the number of pollen grains stained red with acetic carmine (2%) solution (Kearns and Inouye, 1993). Anthers from the flower buds were dissected, and pollen was extracted with 500 μL of 0.5 M sucrose, pelleted, resuspended in 200 μL, deposited on a microscope slide, and stained. The number of pollen grains was counted in 10 randomly selected fields per slide. The percentage of pollen fertility was obtained using (number of viable pollen grains)/(number of total pollen grains counted × 100).

Pollen germination tests were performed on glass slides coated with germination medium [0.292 M sucrose, 1.27 mM $Ca(NO_3)_2$, 1.62 mM H_3BO_3,1 mM KH_2PO_4, and 0.5% agarose]. The number of germinated pollen grains was counted with a microscope after 2 h of incubation at 25 °C in the dark. The pollens were observed using a bright field microscope (Zeiss, Axioplan) and photographed with a CCD camera (Motic 3 megapixels). The percentage of pollen germination was obtained using germination (number of germinated pollen grains)/(number of total pollen grains counted × 100).

Scanning transmission electron microscopy (STEM)

Pollen grains from *slsamba* and WT plants were prepared for STEM. After air-drying, the pollen grains were mounted on a sample plate and coated with a 20 nm-thick layer of gold using a Hummer VII-Sputter facility (Analtech). Subsequently, the samples were examined under a ZEISS Gemini SEM 300 scanning electron microscope operating at 30 kV. Image acquisition was performed using a Mamiya RB67 camera connected to the microscope.

Fruit growth parameters and cytological analysis

Fruits from 12 plants per genotype were harvested at anthesis, at 10-, 15-, 20-, 25-, and 30 DPA, and at the RR stage. Fruits were weighed on a semi-analytical scale and imaged with a Nikon D5300 camera before being cut at the equatorial region. The pictures were analyzed with ImageJ (https://imagej.nih.gov/ij/) software to measure fruit diameters, fruit height, and pericarp thickness. Fruit diameters were measured at the equatorial region (D_{eq}) in two directions and averaged. The shape index was calculated as the ratio of fruit height and fruit D_{eq}. The pericarp thickness corresponds to the average of six measurements distributed around the equatorial section. Per genotype, 24 biological replicates (fruits) were analyzed. Equatorial pericarp fragments were fixed in FAA (formaldehyde 4%, ethanol 50%, acetic acid 5%) by applying a strong vacuum of 400 mmHg for 15 min. The fixative was renewed, and the samples were incubated overnight at 4 °C. Pericarps were sliced at 150 μm thickness using an HM 650 V Vibrating-Blade Microtome (Thermo Scientific). The sections were transferred to phosphate buffer saline (PBS, consisting of 137 mM NaCl, 2.7 mM KCl, 10 mM Na_2HPO_4, 1.8 mM KH_2PO_4, pH 7). PBS was replaced by a PBS-staining solution containing 4′,6-diamidino-2-phenylindole (DAPI) at 20 μg/mL and calcofluor white at 1.33 μg/mL following incubation for 15 min. After three washes of 5 min with PBS, the sections were mounted with Citifluor AF1™ (Electron Microscopy Science) to reduce fluorescence fading. Sections were imaged with a Zeiss LSM880 confocal laser scanning microscope using a 20x dry objective (NA 0.8). For calcofluor and DAPI visualization, excitation was performed at 405 nm, and fluorescence emission was collected at 420–480 nm. Cell walls were manually outlined using SketchBook software, and cell size was determined using Image J. The number of cell layers was counted.

Ovary growth parameters and cytological analysis

Flowers at anthesis and stage 11 (4 mm) (Brukhin *et al*., 2003) from 24 plants per genotype were harvested. The perianth and anthers were removed, keeping the ovary fixed on the peduncle to facilitate manipulation. Pictures were taken to measure

diameter and length, and then samples were immediately immersed in FAA by applying a vacuum of 350 mmHg for 15 min. The fixative solution was renewed, and samples were incubated overnight at 4 °C. Samples were dehydrated using an ethanol series (70, 96, 100%), transferred to histosol, and finally embedded in paraffin wax. Ovaries were sectioned (8 μm thick) in longitudinal and transversal directions and stained with 0.1% toluidine blue. Slices were imaged with an Axiozoom macroscope (Zeiss) and analyzed with ImageJ software. Three regions of each ovary wall were analyzed for measuring thickness, counting the number of cell layers, and measuring the cell size. The average cell size was determined by the ratio of a selected area to the number of cells.

Ploidy level analysis

Frozen equatorial sections of fruit pericarps (*slsamba* and WT) of 0, 3, 5, 10, 15, 20, 25, 30 DPA, and red ripe were chopped with a razor blade into 400 μL of chilled CyStain UV Precise P Nuclei Extraction Buffer (Sysmex). The suspension was filtered through a 50 μm nylon filter, and 1600 μL of chilled CyStain UV Precise P Staining Buffer (Sysmex) was added to the isolated nuclei. The nuclei DNA content was measured using a 208 CyFlow 9 Space flow cytometer (Sysmex). Ploidy profiles were then analyzed with FloMax software (Sysmex). The percentage of all ploidy levels was calculated from the raw count obtained through the gating region of each peak. The 2C nuclei in the 30 DPA and red ripe stages were set to zero as the corresponding peaks were in the background noise. The mean C value (MCV) defined as the sum of each C value class weighed by their frequency, was calculated (Cheniclet *et al*., 2005).

Fruit quality

Red ripe fruits (52 DPA, 24 fruits per genotype) were homogenized and the total soluble solids (°Brix) of the resulting juices were measured with a digital Brix refractometer (ATAGO PAL-BX/ACID3).

Extraction and analysis of metabolites

Metabolite analyses were performed in fruits from WT and individual homozygous *slsamba* plants (lines 3 and 27) harvested at different developmental stages (3, 5, 8, and 52 DPA). Pools of 10 fruits were collected, immediately frozen in liquid nitrogen, powdered, and stored at −80 °C until extraction.

Extraction and quantification of primary and secondary metabolites (4–7 replicates) were performed as described by Salem *et al*. (2016). Briefly, 150 and 300 μL of the polar phase were dried in a centrifugal vacuum concentrator for primary and secondary metabolite profiling, respectively. The primary metabolite pellet was resuspended in 40 μL methoxyaminhydrochloride (20 mg mL^{-1} in pyridine) and derivatized for 2 h at 37 °C. Afterwards, 70 μL of N-methyl-N-[trimethylsilyl] trifluoroacetamide containing a 20 μL mL^{-1} fatty acid methyl esters mixture as retention time standards were added. The mixture was incubated for 30 min at 37 °C at 400 rpm shaking. A volume of 1 μL of this solution was injected into an Agilent 6890 N gas chromatograph coupled with a LECO Pegasus III time-of-flight mass spectrometry (TOF-MS) running in electron ionization (EI).

The secondary metabolite pellet was resuspended in 200 μL of 50% (v/v) methanol in water, and 2 mL was injected into an RP high-strength silica T3 C18 column using a Waters Acquity UPLC system. The analysis workflow included peak detection, retention time alignment, and removal of chemical noise. PLS-DA and heat map analysis were performed by MetaboAnalyst 6.0 (https://www.metaboanalyst.ca/).

RNA-seq

RNA-seq analysis was performed on three pools of the same samples analyzed for primary and secondary metabolites. Total RNA was isolated using TRIzol (ThermoFisher, USA) according to the manufacturer's instructions, purified and quantified with a NanoDrop 2000 spectrophotometer (Thermo Scientific, USA) and Qubit, and its integrity was examined by electrophoresis. To eliminate the residual genomic DNA present in the preparation, the RNA was treated by RNAse-free DNase I according to the manufacturer's instructions (Promega, USA).

RNA samples were sent to the NGS services Fasteris Co., Ltd. (Switzerland) for sequencing. The sequencing libraries were prepared with the Illumina TruSeq stranded mRNA kit and sequenced in 150 bp paired-end mode in NovaSeq 6000. At least 50 million read pairs were obtained for each sample. Each sequencing library was then processed with *fastp v.0.23.4* (Chen *et al*., 2018) to remove adapters, poly-A tails, reads with more than 20% bases below Phred quality of 30, reads smaller than 100 bp, and larger than 150 bp. The libraries' strandedness was checked with the software *how_are_we_stranded_here v.1.0.1* (https://github.com/signalbash/how_are_we_stranded_here) before quantification.

Transcript quantification was performed with *Salmon v.1.10.0* (Patro *et al*., 2017) using the gentrome as a reference, a combination of the transcripts (ITAG4.1) and genomic (SL4.0) sequences where the latter are used as decoys to avoid mismapping. From this point forward, the analyzes were performed individually for each time point. The quantification files were imported into R version 4.4.1 with the package *tximport 1.32.0* (Soneson *et al*., 2015) to generate transcript- and gene-level count tables. Since ITAG4.1 only provides a single transcript per gene, all analyzes were performed at the gene level. Genes with low expression were filtered from the count table with a cutoff of 1 CPM in at least three samples. Then, the filtered counts were normalized by TMM (Robinson and Oshlack, 2010), and the mean–variance relationships for each gene were calculated with voom using sample weights to account for sample heterogeneity (Liu *et al*., 2015). The limma package was used to fit a linear model, apply contrasts between the genotypes, and adjust variance estimates (Ritchie *et al*., 2015). The results of the DE analysis were filtered by choosing an adjusted *P*-value <0.05 and an absolute log2(fold-change) of 1.5.

For metabolite-gene correlation analyzes, the average normalized expression values of genes and metabolites at each time point were used. Then, Spearman's correlation coefficient was calculated using R version 4.4.1. Correlation values (ρ) above 0.75 and below −0.75 were considered relevant for interpreting the results.

TF-binding site enrichment analysis

Enrichment analysis for TF-binding sites (TFBS; or motifs), in 2-kb sequences upstream from the translation start site of the *slsamba* DEGs, was performed essentially as described by Gryffroy *et al*. (2023a). Where needed, the upstream sequences were shortened to avoid overlap with neighbouring genes. Known motifs for tomato were collected from CisBP version 2.00 (Weirauch *et al*., 2014) and JASPAR 2020 (Fornes *et al*., 2020). These motifs were mapped onto the 2-kb sequences upstream of *slsamba* DEGs using FIMO (MEME version 4.11.4; default

parameters) (Grant *et al*., 2011) and Cluster-Buster (compiled on September 22, 2017) (Frith *et al*., 2003) with the cluster score threshold (−c) set to 0. Following Kulkarni *et al*. (2019), the 7000 top-scoring motif matches from FIMO were combined with the 4000 top-scoring matches from Cluster-Buster, and lower-scoring matches were discarded. Within each set of DEGs, a hypergeometric test was performed per motif, and all motifs with Benjamini-Hochberg adjusted *P*-value <0.05 were considered enriched within that DEG set. To focus on motifs that are specifically enriched in the set of up- or down-regulated genes at a certain time point, the set of expressed genes (with known motifs in their 2-kb upstream sequence) at that time point was used as background for the hypergeometric tests. To sort enriched motifs, taking into account both statistical significance (adjusted *P*-value) and enrichment fold, π-values were computed following Xiao *et al*. (2014). Enriched motifs were sorted decreasingly by π-values.

Statistical analysis

All values were expressed as the mean ± standard error of the mean (SEM). Data from lines *slsamba* and WT plants were analyzed with ANOVA and Dunnett's tests using GraphPad Prism 5 software (La Jolla, CA). Probabilities of $P < 0.05$ and $P < 0.01$ were considered statistically significant.

Acknowledgements

We thank Sandra Pedemay for technical assistance during the analysis of electron micrographs and all the members of the Flowering, Fruit Development and Environmental Constraints – FDFE for helpful discussions. We thank Isabelle Atienza-Babin for helping with the propagation of the mutant lines. This research was supported by the São Paulo Research Foundation (FAPESP), NBE 2017/10333-8, PNO 2021/06611-8, LFCS 2021/03212-5, AIC 23/13107-0, and MLSS 20/00888-5.

Conflict of interest

The authors have no conflict of interest to declare.

Author contributions

N.B.E. designed the project. P.N.O., L.P.S., P.B.F., J.P.M., L.F.C.S., A.I.C., M.L.S.S., S.S.G., H.B., L.R.S., and L.E.P. performed the experiments. M.C.M.M., N.B., L.E.P.P., K.V., A.G., N.G., and A.R.F. provided technical support and intellectual input. P.N.O., P.B.F., and N.B.E. wrote the manuscript. All authors read and approved the final manuscript.

Data availability statement

The data that supports the findings of this study are available in the supplementary material of this article.

References

Alfieri, C., Chang, L., Zhang, Z., Yang, J., Maslen, S., Skehel, M. and Barford, D. (2016) Molecular basis of APC/C regulation by the spindle assembly checkpoint. *Nature* **536**, 431–436.

Alfieri, C., Zhang, S. and Barford, D. (2017) Visualizing the complex functions and mechanisms of the anaphase promoting complex/cyclosome (APC/C). *Open Biol.* **7**, 170204.

Arora, D., Abel, N.B., Liu, C., Van Damme, P., Yperman, K., Eeckhout, D., Vu, L.D. *et al*. (2020) Establishment of Proximity-Dependent Biotinylation Approaches in Different Plant Model Systems. *Plant Cell* **32**, 3388–3407.

Baker, D.J., Dawlaty, M.M., Galardy, P. and van Deursen, J.M. (2007) Mitotic regulation of the anaphase-promoting complex. *Cell Mol. Life Sci.* **64**, 589–600.

Beauvoit, B.P., Colombié, S., Monier, A., Andrieu, M.H., Biais, B., Bénard, C., Chéniclet, C. *et al*. (2014) Model-assisted analysis of sugar metabolism throughout tomato fruit development reveals enzyme and carrier properties in relation to vacuole expansion. *Plant Cell* **26**, 3224–3242.

Biais, B., Bénard, C., Beauvoit, B., Colombié, S., Prodhomme, D., Ménard, G., Bernillon, S. *et al*. (2014) Remarkable reproducibility of enzyme activity profiles in tomato fruits grown under contrasting environments provides a roadmap for studies of fruit metabolism. *Plant Physiol.* **164**, 1204–1221.

Blilou, I., Frugier, F., Folmer, S., Serralbo, O., Willemsen, V., Wolkenfelt, H., Eloy, N.B. *et al*. (2002) The Arabidopsis HOBBIT gene encodes a CDC27 homolog that links the plant cell cycle to progression of cell differentiation. *Genes Dev.* **16**, 2566–2575.

Bolaños-Villegas, P., Xu, W., Martínez-García, M., Pradillo, M. and Wang, Y. (2018) Insights into the role of ubiquitination in meiosis: Fertility, adaptation and plant breeding. *The Arabidopsis Book* **16**, e0187.

Braun, D.M. (2022) Phloem Loading and Unloading of Sucrose: What a Long, Strange Trip from Source to Sink. *Annu. Rev. Plant Biol.* **73**, 553–584.

Brukhin, V., Hernould, M., Gonzalez, N., Chevalier, C. and Mouras, A. (2003) Flower development schedule in tomato (Lycopersicon esculentum cv. Sweet Cherry). *Sex. Plant Reprod.* **15**, 311–320.

Buschhorn, B.A. and Peters, J.M. (2006) How APC/C orders destruction. *Nat. Cell Biol.* **8**, 209–211.

Capron, A., Serralbo, O., Fülöp, K., Frugier, F., Parmentier, Y., Dong, A., Lecureuil, A. *et al*. (2003) The Arabidopsis anaphase-promoting complex or cyclosome: molecular and genetic characterization of the APC2 subunit. *Plant Cell* **15**, 2370–2382.

Chen, S., Zhou, Y., Chen, Y. and Gu, J. (2018) fastp: An ultra-fast all-in-one FASTQ preprocessor. *Bioinformatics* **34**, i884–i890.

Chen, T., Zhang, Z., Li, B., Qin, G. and Tian, S. (2021) Molecular basis for optimizing sugar metabolism and transport during fruit development. *aBIOTECH* **2**, 330–340.

Cheniclet, C., Rong, W.Y., Causse, M., Frangne, N., Bolling, L., Carde, J.P. and Renaudin, J.P. (2005) Cell expansion and endoreduplication show a large genetic variability in pericarp and contribute strongly to tomato fruit growth. *Plant Physiol.* **139**, 1984–1994.

Chiocchio, I., Andrés, N.P., Anaia, R.A., van Dam, N.M. and Vergara, F. (2023) Steroidal glycoside profile differences among primary roots system and adventitious roots in Solanum dulcamara. *Planta* **257**, 37.

Cuéllar, A.P., Pauwels, L., De Clercq, R. and Goossens, A. (2013) Yeast two-hybrid analysis of jasmonate signaling proteins. *Methods Mol. Biol.* **1011**, 173–185.

Dali, N., Michaud, D. and Yelle, S. (1992) Evidence for the involvement of sucrose phosphate synthase in the pathway of sugar accumulation in sucrose-accumulating tomato fruits. *Plant Physiol.* **99**, 434–438.

D'Andrea, L.D. and Regan, L. (2003) TPR proteins: The versatile helix. *Trends Biochem. Sci.* **28**, 655–662.

d'Erfurth, I., Jolivet, S., Froger, N., Catrice, O., Novatchkova, M. and Mercier, R. (2009) Turning meiosis into mitosis. *PLoS Biol.* **7**, e1000124.

Dirick, L., Böhm, T. and Nasmyth, K. (1995) Roles and regulation of Cln-Cdc28 kinases at the start of the cell cycle of Saccharomyces cerevisiae. *EMBO J.* **14**, 4803–4813.

Eloy, N.B., de Freitas Lima, M., Van Damme, D., Vanhaeren, H., Gonzalez, N., De Milde, L., Hemerly, A.S. *et al*. (2011) The APC/C subunit 10 plays an essential role in cell proliferation during leaf development. *Plant J.* **68**, 351–363.

Eloy, N.B., Gonzalez, N., Van Leene, J., Maleux, K., Vanhaeren, H., De Milde, L., Dhondt, S. *et al*. (2012) SAMBA, a plant-specific anaphase-promoting complex/cyclosome regulator is involved in early development and A-type cyclin stabilization. *Proc. Natl. Acad. Sci.* **109**, 13853–13858.

Eloy, N.B., de Freitas Lima, M., Ferreira, P.C.G. and Inzé, D. (2015) The role of the anaphase-promoting complex/cyclosome in plant growth. *Crit. Rev. Plant Sci.* **34**, 487–505.

Faurobert, M., Mihr, C., Bertin, N., Pawlowski, T., Negroni, L., Sommerer, N. and Causse, M. (2007) Major proteome variations associated with cherry tomato pericarp development and ripening. *Plant Physiol.* **143**, 1327–1346.

Feng, C.Y., Han, J.X., Han, X.X. and Jiang, J. (2015) Genome-wide identification, phylogeny, and expression analysis of the SWEET gene family in tomato. *Gene* **573**, 261–272.

Ferreira e Silva, G.F., Silva, E.M., Azevedo, M.d.S., Guivin, M.A., Ramiro, D.A., Figueiredo, C.R., Carrer, H. *et al*. (2014) microRNA156-targeted SPL/SBP box transcription factors regulate tomato ovary and fruit development. *Plant J.* **78**, 604–618.

Fornes, O., Castro-Mondragon, J.A., Khan, A., van der Lee, R., Zhang, X., Richmond, P.A., Modi, B.P. *et al*. (2020) JASPAR 2020: Update of the open-access database of transcription factor binding profiles. *Nucleic Acids Res.* **48** (D1), D87–D92.

Frandsen, J.R. and Narayanasamy, P. (2018) Neuroprotection through flavonoid: Enhancement of the glyoxalase pathway. *Redox Biol.* **14**, 465–473.

Fridman, E., Carrari, F., Liu, Y.S., Fernie, A.R. and Zamir, D. (2004) Zooming in on a quantitative trait for tomato yield using interspecific introgressions. *Science* **305**, 1786–1789.

Frith, M.C., Li, M.C. and Weng, Z. (2003) Cluster-Buster: Finding dense clusters of motifs in DNA sequences. *Nucleic Acids Res.* **31**, 3666–3668.

Galili, G., Amir, R. and Fernie, A.R. (2016) The Regulation of Essential Amino Acid Synthesis and Accumulation in Plants. *Annu. Rev. Plant Biol.* **67**, 153–178.

Gao, F. and Dubos, C. (2024) The arabidopsis bHLH transcription factor family. *Trends Plant Sci.* **29**, 668–680.

Giovannucci, E. (1999) Tomatoes, tomato-based products, lycopene, and cancer: Review of the epidemiologic literature. *J. Natl. Cancer Inst.* **91**, 317–331.

Gong, P., Bontinck, M., Demuynck, K., De Block, J., Gevaert, K., Eeckhout, D., Persiau, G. *et al*. (2022) SAMBA controls cell division rate during maize development. *Plant Physiol.* **188**(1), 411–424.

Grant, C.E., Bailey, T.L. and Noble, W.S. (2011) FIMO: Scanning for occurrences of a given motif. *Bioinformatics* **27**, 1017–1018.

Gryffroy, L., De Ryck, J., Jonckheere, V., Goormachtig, S., Goossens, A. and Van Damme, P. (2023a) Cataloguing Protein Complexes In Planta Using TurboID-Catalyzed Proximity Labeling. *Methods Mol. Biol.* **2690**, 311–334.

Gryffroy, L., Ceulemans, E., Manosalva Pérez, N., Venegas-Molina, J., Jaramillo-Madrid, A.C., Rodrigues, S.D., De Milde, L. *et al*. (2023b) Rhizogenic Agrobacterium protein RolB interacts with the TOPLESS repressor proteins to reprogram plant immunity and development. *Proc. Natl. Acad. Sci.* **120**, e2210300120.

Guo, L., Jiang, L., Zhang, Y., Lu, X.L., Xie, Q., Weijers, D. and Liu, C.M. (2016) The anaphase-promoting complex initiates zygote division in Arabidopsis through degradation of cyclin B1. *Plant J.* **86**(2), 161–174.

Guo, L., Jiang, L., Lu, X.L. and Liu, C.M. (2018) ANAPHASE PROMOTING COMPLEX/CYCLOSOME-mediated cyclin B1 degradation is critical for cell cycle synchronization in syncytial endosperms. *J. Integr. Plant Biol.* **60**, 448–454.

Hao, Y., Zong, X., Ren, P., Qian, Y. and Fu, A. (2021) Basic Helix-Loop-Helix (bHLH) Transcription Factors Regulate a Wide Range of Functions in Arabidopsis. *Int. J. Mol. Sci.* **22**, 7152.

Harper, J.W., Burton, J.L. and Solomon, M.J. (2002) The anaphase-promoting complex: it's not just for mitosis any more. *Genes Dev.* **16**, 2179–2206.

Heyman, J., Van den Daele, H., De Wit, K., Boudolf, V., Berckmans, B., Verkest, A., Alvim Kamei, C.L. *et al*. (2011) Arabidopsis ULTRAVIOLET-B-INSENSITIVE4 maintains cell division activity by temporal inhibition of the anaphase-promoting complex/cyclosome. *Plant Cell* **23**, 4394–4410.

Hirano, H., Harashima, H., Shinmyo, A. and Sekine, M. (2008) Arabidopsis RETINOBLASTOMA-RELATED PROTEIN 1 is involved in G1 phase cell cycle arrest caused by sucrose starvation. *Plant Mol. Biol.* **66**, 259–275.

Hirano, H., Shinmyo, A. and Sekine, M. (2011) Arabidopsis G1 cell cycle proteins undergo proteasome-dependent degradation during sucrose starvation. *Plant Physiol. Biochem.* **49**, 687–691.

Ho, L.C. (1996) Tomato. In *Photoassimilate Distribution in Plant and Crops* (Zamki, E. and Shaffer, A.A., eds), pp. 709–728. New York: Marcel Dekker, Inc.

Inzé, D. and Nelissen, H. (2022) The translatability of genetic networks from model to crop species: lessons from the past and perspectives for the future. *New Phytol.* **236**, 43–48.

Iwata, E., Ikeda, S., Matsunaga, S., Kurata, M., Yoshioka, Y., Criqui, M.C., Genschik, P. *et al*. (2011) GIGAS CELL1, a novel negative regulator of the anaphase-promoting complex/cyclosome, is required for proper mitotic progression and cell fate determination in Arabidopsis. *Plant Cell* **23**, 4382–4393.

Julius, B.T., Leach, K.A., Tran, T.M., Mertz, R.A. and Braun, D.M. (2017) Sugar Transporters in Plants: New Insights and Discoveries. *Plant Cell Physiol.* **58**, 1442–1460.

Kearns, C.A. and Inouye, D. (1993) *Techniques for pollinations biologists*. Niwot: University Press of Colorado.

Kulkarni, S.R., Jones, D.M. and Vandepoele, K. (2019) Enhanced Maps of Transcription Factor Binding Sites Improve Regulatory Networks Learned from Accessible Chromatin Data. *Plant Physiol.* **181**, 412–425.

Kumar, M., Basha, P.O., Puri, A., Rajpurohit, D., Randhawa, G.S., Sharma, T.R. and Dhaliwal, H.S. (2010) A candidate gene OsAPC6 of anaphase-promoting complex of rice identified through T-DNA insertion. *Funct. Integr. Genomics* **10**, 349–358.

Kuppusamy, K.T., Ivashuta, S., Bucciarelli, B., Vance, C.P., Gantt, J.S. and Vandenbosch, K.A. (2009) Knockdown of CELL DIVISION CYCLE16 reveals an inverse relationship between lateral root and nodule numbers and a link to auxin in Medicago truncatula. *Plant Physiol.* **151**, 1155–1166.

Kwee, H.S. and Sundaresan, V. (2003) The NOMEGA gene required for female gametophyte development encodes the putative APC6/CDC16 component of the Anaphase Promoting Complex in Arabidopsis. *Plant J.* **36**(6), 853–866.

Lin, Q., Wang, D., Dong, H., Gu, S., Cheng, Z., Gong, J., Qin, R. *et al*. (2012) Rice APC/C(TE) controls tillering by mediating the degradation of MONOCULM 1. *Nat. Commun.* **3**, 752.

Liu, H.F., Génard, M., Guichard, S. and Bertin, N. (2007) Model-assisted analysis of tomato fruit growth in relation to carbon and water fluxes. *J. Exp. Bot.* **58** (13), 3567–3580.

Liu, R., Holik, A.Z., Su, S., Jansz, N., Chen, K., Leong, H.S., Blewitt, M.E. *et al*. (2015) Why weight? Modelling sample and observational level variability improves power in RNA-seq analyses. *Nucleic Acids Res.* **43**, e97.

Livak, K.J. and Schmittgen, T.D. (2001) Analysis of relative gene expression data using real-time quantitative PCR and the $2(-\Delta\Delta CT)$ method. *Methods* **25**, 402–408.

Marrocco, K., Thomann, A., Parmentier, Y., Genschik, P. and Criqui, M.C. (2009) The APC/C E3 ligase remains active in most post-mitotic Arabidopsis cells and is required for proper vasculature development and organization. *Development* **136**, 1475–1485.

Martin, C. and Li, J. (2017) Medicine is not health care, food is health care: Plant metabolic engineering, diet, and human health. *New Phytol.* **216**, 699–719.

Mauxion, J.P., Chevalier, C. and Gonzalez, N. (2021) Complex cellular and molecular events determining fruit size. *Trends Plant Sci.* **26**, 1023–1038.

Menges, M., Samland, A.K., Planchais, S. and Murray, J.A. (2006) The D-type cyclin CYCD3;1 is limiting for the G1-to-S-phase transition in Arabidopsis. *Plant Cell* **18**(4), 893–906.

Moing, A., Berton, T., Roch, L., Diarrassouba, S., Bernillon, S., Arrivault, S., Deborde, C. *et al*. (2023) Multi-omics quantitative data of tomato fruit unveils regulation modes of least variable metabolites. *BMC Plant Biol.* **23**, 365.

Mumtaz, M.A., Li, F., Zhang, X., Tao, J., Ge, P., Wang, Y., Wang, Y. *et al*. (2022) Altered brassinolide sensitivity1 regulates fruit size in association with phytohormones modulation in tomato. *Horticulturae* **8**, 1008.

Nguyen, T.H., Thiers, L., Van Moerkercke, A., Bai, Y., Fernández-Calvo, P., Minne, M., Depuydt, T. *et al*. (2023) A redundant transcription factor network steers spatiotemporal Arabidopsis triterpene synthesis. *Nature Plants* **9**, 926–937.

Obiadalla-Ali, H., Fernie, A.R., Kossmann, J. and Lloyd, J.R. (2004) Developmental analysis of carbohydrate metabolism in tomato (Lycopersicon esculentum cv. Micro-Tom) fruits. *Physiol. Plant.* **120**, 196–204.

Patrick, J.W. (1997) PHLOEM UNLOADING: sieve element unloading and post-sieve element transport. *Annu. Rev. Plant Physiol. Plant Mol. Biol.* **48**, 191–222.

Patro, R., Duggal, G., Love, M.I., Irizarry, R.A. and Kingsford, C. (2017) Salmon provides fast and bias-aware quantification of transcript expression. *Nat. Methods* **14**, 417–419.

Pérez-Pérez, J.M., Serralbo, O., Vanstraelen, M., González, C., Criqui, M.C., Genschik, P., Kondorosi, E. *et al*. (2008) Specialization of CDC27 function in the *Arabidopsis thaliana* anaphase-promoting complex (APC/C). *Plant J.* **53** (1), 78–89.

Peters, J.M. (2002) The anaphase-promoting complex: proteolysis in mitosis and beyond. *Mol. Cell* **9**, 931–943.

Petersen, B.O., Wagener, C., Marinoni, F., Kramer, E.R., Melixetian, M., Lazzerini Denchi, E., Gieffers, C. *et al*. (2000) Cell cycle- and cell growth-regulated proteolysis of mammalian CDC6 is dependent on APC-CDH1. *Genes Dev.* **14**, 2330–2343.

Pino, L.E., Lombardi-Crestana, S., Azevedo, M.S., Scotton, D.C., Borgo, L., Quecini, V., Figueira, A. *et al*. (2010) The Rg1 allele as a valuable tool for genetic transformation of the tomato 'Micro-Tom' model system. *Plant Methods* **6**, 23.

Quinet, M., Angosto, T., Yuste-Lisbona, F.J., Blanchard-Gros, R., Bigot, S., Martinez, J.P. and Lutts, S. (2019) Tomato fruit development and metabolism. *Front. Plant Sci.* **10**, 1554.

Rawat, S.S. and Laxmi, A. (2024) Sugar signals pedal the cell cycle! *Front. Plant Sci.* **15**, 1354561.

Ren, H., Santner, A., del Pozo, J.C., Murray, J.A. and Estelle, M. (2008) Degradation of the cyclin-dependent kinase inhibitor KRP1 is regulated by two different ubiquitin E3 ligases. *Plant J.* **53**, 705–716.

Reuscher, S., Akiyama, M., Yasuda, T., Makino, H., Aoki, K., Shibata, D. and Shiratake, K. (2014) The sugar transporter inventory of tomato: genome-wide identification and expression analysis. *Plant Cell Physiol.* **55**(6), 1123–1141.

Riou-Khamlichi, C., Menges, M., Healy, J.M. and Murray, J.A. (2000) Sugar control of the plant cell cycle: differential regulation of Arabidopsis D-type cyclin gene expression. *Mol. Cell. Biol.* **20**(13), 4513–4521.

Ritchie, M.E., Phipson, B., Wu, D., Hu, Y., Law, C.W., Shi, W. and Smyth, G.K. (2015) limma powers differential expression analyses for RNA-sequencing and microarray studies. *Nucleic Acids Res.* **43**, e47.

Robinson, M.D. and Oshlack, A. (2010) A scaling normalization method for differential expression analysis of RNA-seq data. *Genome Biol.* **11**, R25.

Rojas, C.A., Eloy, N.B., Lima, M.d.F., Rodrigues, R.L., Franco, L.O., Himanen, K., Beemster, G.T. *et al*. (2009) Overexpression of the Arabidopsis anaphase promoting complex subunit CDC27a increases growth rate and organ size. *Plant Mol. Biol.* **71**, 307–318.

Ruan, Y.L. and Patrick, J.W. (1995) The cellular pathway of post phloem sugar transport in developing tomato fruit. *Planta* **196**, 434–444.

Salem, M.A., Jüppner, J., Bajdzienko, K. and Giavalisco, P. (2016) Protocol: A fast, comprehensive, and reproducible one-step extraction method for the rapid preparation of polar and semi-polar metabolites, lipids, proteins, starch, and cell wall polymers from a single sample. *Plant Methods* **12**, 45.

Saze, H. and Kakutani, T. (2007) Heritable epigenetic mutation of a transposon-flanked Arabidopsis gene due to lack of the chromatin-remodeling factor DDM1. *EMBO J.* **26**, 3641–3652.

Schwedersky, R.P., Saleme, M.L.S., Rocha, I.A., Montessoro, P.D.F., Hemerly, A.S., Eloy, N.B. and Ferreira, P.C.G. (2021) The Anaphase Promoting Complex/Cyclosome Subunit 11 and Its Role in Organ Size and Plant Development. *Front. Plant Sci.* **12**, 563760.

Sekhon, R.S., Lin, H.N., Childs, K.L., Hansey, C.N., Buell, C.R., de Leon, N. and Kaeppler, S.M. (2011) Genome-wide atlas of transcription during maize development. *Plant J.* **66**, 553–563.

Seymour, G.B., Chapman, N.H., Chew, B.L. and Rose, J.K. (2013) Regulation of ripening and opportunities for control in tomato and other fruits. *Plant Biotechnol. J.* **11**, 269–278.

Smeekens, S., Ma, J., Hanson, J. and Rolland, F. (2010) Sugar signals and molecular networks controlling plant growth. *Curr. Opin. Plant Biol.* **13**, 274–279.

Soneson, C., Love, M.I. and Robinson, M.D. (2015) Differential analyses for RNA-seq: Transcript-level estimates improve gene-level inferences. *F1000Res* **4**, 1521.

Sprunck, S. (2020) Twice the fun, double the trouble: gamete interactions in flowering plants. *Curr. Opin. Plant Biol.* **53**, 106–116.

Sun, L., Wang, J., Lian, L., Song, J., Du, X., Liu, W., Zhao, W. *et al*. (2022) Systematic analysis of the sugar accumulation mechanism in sucrose- and hexose-accumulating cherry tomato fruits. *BMC Plant Biol.* **22**, 303.

Thompson, J.D., Gibson, T.J., Plewniak, F., Jeanmougin, F. and Higgins, D.G. (1997) The CLUSTAL_X windows interface: flexible strategies for multiple sequence alignment aided by quality analysis tools. *Nucleic Acids Res.* **25**, 4876–4882.

Thornton, B.R. and Toczyski, D.P. (2003) Securin and B-cyclin/CDK are the only essential targets of the APC. *Nat. Cell Biol.* **5**, 1090–1094.

Thornton, B.R., Ng, T.M., Matyskiela, M.E., Carroll, C.W., Morgan, D.O. and Toczyski, D.P. (2006) An architectural map of the anaphase-promoting complex. *Genes Dev.* **20**, 449–460.

Verkest, A., Manes, C.L., Vercruysse, S., Maes, S., Van Der Schueren, E., Beeckman, T., Genschik, P. *et al*. (2005) The cyclin-dependent kinase inhibitor KRP2 controls the onset of the endoreduplication cycle during Arabidopsis leaf development through inhibition of mitotic CDKA;1 kinase complexes. *Plant Cell* **17**, 1723–1736.

Waese, J., Fan, J., Pasha, A., Yu, H., Fucile, G., Shi, R., Cumming, M. *et al*. (2017) ePlant: Visualizing and exploring multiple levels of data for hypothesis generation in plant biology. *Plant Cell* **29**, 1806–1821.

Wang, L. and Ruan, Y.-L. (2013) Regulation of cell division and expansion by sugar and auxin signaling. *Front. Plant Sci.* **4**, 163.

Wang, Y., Hou, Y., Gu, H., Kang, D., Chen, Z., Liu, J. and Qu, L.J. (2012) The Arabidopsis APC4 subunit of the anaphase-promoting complex/cyclosome (APC/C) is critical for both female gametogenesis and embryogenesis. *Plant J.* **69**, 227–240.

Wang, Y., Zhong, Z., Zhang, Y., Xu, L., Feng, S., Rayatpisheh, S., Wohlschlegel, J.A. *et al*. (2020) NAP1-RELATED PROTEIN1 and 2 negatively regulate H2A. Z abundance in chromatin in Arabidopsis. *Nat. Commun.* **11**(1), 2887.

Weirauch, M.T., Yang, A., Albu, M., Cote, A.G., Montenegro-Montero, A., Drewe, P., Najafabadi, H.S. *et al*. (2014) Determination and inference of eukaryotic transcription factor sequence specificity. *Cell* **158**, 1431–1443.

Willcox, J.K., Catignani, G.L. and Lazarus, S. (2003) Tomatoes and cardiovascular health. *Crit. Rev. Food Sci. Nutr.* **43**, 1–18.

Wu, S., Zhang, B., Keyhaninejad, N., Rodríguez, G.R., Kim, H.J., Chakrabarti, M., Illa-Berenguer, E. *et al*. (2018) A common genetic mechanism underlies morphological diversity in fruits and other plant organs. *Nat. Commun.* **9**(1), 4734.

Xiao, H., Jiang, N., Schaffner, E., Stockinger, E.J. and van der Knaap, E. (2008) A retrotransposon-mediated gene duplication underlies morphological variation of tomato fruit. *Science* **319**(5869), 1527–1530.

Xiao, Y., Hsiao, T.H., Suresh, U., Chen, H.I., Wu, X., Wolf, S.E. and Chen, Y. (2014) A novel significance score for gene selection and ranking. *Bioinformatics* **30**, 801–807.

Yelle, S., Hewitt, J.D., Robinson, N.L., Damon, S. and Bennett, A.B. (1988) Sink metabolism in tomato fruit III: Analysis of carbohydrate assimilation in a wild species. *Plant Physiol.* **87**, 737–740.

Zhang, Y., Butelli, E., Alseekh, S., Tohge, T., Rallapalli, G., Luo, J., Kawar, P.G. *et al*. (2015) Multi-level engineering facilitates the production of phenylpropanoid compounds in tomato. *Nat. Commun.* **6**, 8635.

Zhang, S., Xu, M., Qiu, Z., Wang, K., Du, Y., Gu, L. and Cui, X. (2016) Spatiotemporal transcriptome provides insights into early fruit development of tomato (Solanum lycopersicum). *Sci. Rep.* **6**, 23173.

Zhang, Y., Chen, M., Siemiatkowska, B., Toleco, M.R., Jing, Y., Strotmann, V., Zhang, J. *et al*. (2020) A Highly Efficient Agrobacterium-Mediated Method for Transient Gene Expression and Functional Studies in Multiple Plant Species. *Plant commun.* **1**, 100028.

Zhang, K., Li, Y., Huang, T. and Li, Z. (2022) Potential application of TurboID-based proximity labeling in studying the protein interaction network in plant response to abiotic stress. *Front. Plant Sci.* **13**, 974598.

Zhang, J., Lyu, H., Chen, J., Cao, X., Du, R., Ma, L., Wang, N. *et al*. (2024) Releasing a sugar brake generates sweeter tomato without yield penalty. *Nature* **635**, 647–656.

Supporting information

Additional supporting information may be found online in the Supporting Information section at the end of the article.

Figure S1 Plant BAR eFP browser showing the expression of *SAMBA* (*Solyc08g076580*) in distinct tomato tissues.
Figure S2 Expression of pSlSAMBA-GUS-GFP and SAMBA:EGFP vectors used for subcellular localization analysis.
Figure S3 Statistical analysis on TurboID samples (SlSAMBA and eGFP) and SlSAMBA interacts with CDC27b in the yeast two-hybrid assay.
Figure S4 Generation of *slsamba* mutants by CRISPR/Cas9.
Figure S5 Phenotypic effect of *slsamba* gene editing on tomato fruit diameter.
Figure S6 Flow cytometry analysis of nuclear DNA ploidy distribution in pericarps of wild-type (WT) and *slsamba* fruits (#3 and #27).
Figure S7 Metabolic characterization of tomato fruit analyzed by GC–MS.
Figure S8 Metabolic characterization of tomato fruit by LC–MS.
Figure S9 Soluble solids (°Brix) of red ripe tomato fruits from *slsamba* lines and wild-type plants.
Figure S10 Differential expression analysis between *slsamba-3* and WT fruits.
Figure S11 Relative expression of genes by qRT-PCR in *slsamba* line 3 and WT fruits harvested at different developmental stages (5-, 8-, and 52 days post anthesis – DPA).
Table S1 Prediction of SlSAMBA subcellular localization by Cello.
Table S2 Transmembrane prediction of the Solyc08g076580.2 (SlSAMBA) protein through the HMMTOP.
Table S3 List of the 41 metabolites identified by GC–MS of fruits at -3, -5, or -8 days post anthesis (DPA) from *slamba* and WT lines.
Table S4 Oligonucleotide sequences used in this work.
Data S1. Significantly enriched protein interactors of SlSAMBA identified by TurboID-mediated proximity labeling in tomato hairy roots.
Data S2. Differential metabolites identified by LC-MS. Data were normalized using Log and Auto-scaling transformations on the MetaboAnalyst platform 6.0.
Data S3. Complete tables of differential expression analysis.
Data S4. MapMan and gene ontology functional enrichment analysis.
Data S5. Annotation and data for sugar transporter genes identified as differentially expressed.
Data S6. Annotation and data for sugar metabolism genes identified as differentially expressed.
Data S7. Motif enrichment analysis on the putative promoters of differentially expressed genes.